Contents

1

Electromagnetic Processing of Materials

The neglected borderland
between two branches of knowledge
is often that which best repays cultivation.

Lord Rayleigh

Steady and time-varying magnetic and electric fields are widely used in various industrial processes involved in the production of materials. This is commonly known as the *Electromagnetic Processing of Materials* (*EPM*). The **interaction of the electromagnetic fields with various media** (liquid and solid metals, liquid semiconductors, plasmas, electrolytes, ferrofluids) occurs by means of various forces, including Lorentz, Kelvin, and diamagnetic forces. This enables materials to be controlled, processed and manipulated thereby affecting their macro and micro-structure [7, 6, 95].

EPM

Although some of the basic principle were recognized more than a century ago, the systematic development and exploitation of these principles is a relatively recent phenomenon, dating from the late 1960's gaining momentum over the last twenty years. The earlier great interest in **Magneto-Hydro-Dynamics** (*MHD*), which was dominated by applications to nuclear fusion research on the one hand and astrophysics on the other hand, spread the whole range of knowledges that is of potentially greatest importance in applied industrial technology [7].

In metal industry, the utilization of the Lorentz's force started very early (electromagnetic levitation in 1923 and electromagnetic mixing in 1932) without enough scientific understanding. In 1982 Alfvén first presented at the Cambridge IUTAM conference the paper "*The Application of Magnetohydrodynamics to Metallurgy*". *EPM* has been established by combining the two channels of **metallurgy** and **MHD**. At first it was growing in the utilization of the Lorentz force mainly relating with the development of steel making processes, especially in a continuous casting. Recently the activity of *EPM* has found another way in the utilization of magnetization force, under the comfortable circumstance where a high magnetic field up to around $10T$ has been easily obtainable thanks to the development of super-conducting technologies [6].

Examples of the action of various forces include magnetic levitation of electrically conducting and non-conducting fluids, melting, stirring, pumping, stabilization of melts, free surfaces and interfaces, etc. *EPM* is involved in the production of metals and alloys (e.g. aluminum, steel, titanium, and magnesium alloys), ceramics crystals and glasses of highest purity, semiconductors (Si, $GaAs$, $CdTe$), and in efficient control of production of nano-scale metallic and ceramic powders, ferro-fluids for medical and engineering applications, laser welding, etc.

EPM is a rapidly developing field but various fundamental issues slow the progress. One of the main reasons for this is complexity of the phenomena involved during the production of materials. A comprehensive approach requires involvement of experts from various branches of materials

science, physics, engineering, and mathematics. As a matter of fact *EPM* is a fully **multi-disciplinary research field**, which involves various topics from Magneto-Hydro-Dynamics (*MHD*), heat and mass transfer, phase transition, metallurgy, electro-chemistry, plasma physics, and other branches of physics, materials science, and engineering.

1.1 *EPM* applications

EPM is by nature an *applied research field*. It relies however on various branches of fundamental research, as theoretical, numerical and experimental studies with the main aim to optimize standard processes and materials or to realize new ones [40]. The following subsections are a global concise description of *EPM* applications where the focus is on the industrial application and the technical future possibilities.

1.1.1 Heat transfer and generation

Heating by electromagnetic sources is an already widely used and applied technology. Using specific frequencies and devices design the heat sources can be generated and distributed in a very efficient way [88].

Different physical phenomena can be involved into heat generation using EM fields. The specific power $w[W/m^3]$ generated by electric current flowing through an electrically conductive materials is expressed by the *Joule's law*: **Joule's law**

$$w = \rho \cdot J^2 \tag{1.1}$$

where $w[W/m^3]$ is the specific heat source, $\rho[\Omega m]$ is the electrical resistivity and $J[A/m^2]$ is the current density modulus. The current density can be a consequence of a direct conduction, or induced from external varying EM field. Almost all metal treatments [89] as surface hardening [125], steels quenching, stress relieving [36], annealing, forging, tempering, etc. can take advantages from *EPM*. Most of the following section examples use in some way this physical principle.

dielectric heating

Analogous for non conductive polar materials in radio-wave or microwave electromagnetic radiation the dipole rotation and excitation generate heat. The *dielectric heating* (RF or microwave heating) specific power $w[W/m^3]$ can be expressed as:

$$w = 2\pi f \cdot \epsilon_0 \cdot \epsilon'' \cdot E^2 \tag{1.2}$$

where $f[Hz]$ is the EM frequency, $\epsilon''[-]$ is the dielectric loss coefficient, ϵ_0 is the vacuum electrical permittivity and $E[V/m]$ the electric field modulus [117, 127].

Examples of the importance of the thermal design, precise control and prediction of the temperature profile are in the **thixo-casting of aluminum** industrial process [45], directional solidification processes (see pag.17 and 49), gears contour hardening, Float Zone silicon production process (see 3.1.2), etc.

1.1.2 Solidification

Solidification occurs in a wide range of industrial applications, including crystal growth and metals casting. The understanding of the solidification processes is based on thermodynamics for describing heat transfer, phase transition phenomena, metallurgical transformations, chemical balances and reactions, as well as on *MHD* for accounting for fluid flows in general and instabilities and turbulence in particular.

The possibility to change the parameters that affect solidification (external electromagnetic fields, mechanical perturbations, thermal gradients, convection, advection, etc.) and its effect on the materials macro and microstructure is a key-point to develop new techniques to improve materials processing. Some specific applications of the interaction between EM fields and solidification will be discussed in details in following sections and chapters.

1.1.3 Mixing and moving liquid conductive materials

It is well known that an alternating magnetic field (either single phase or multiphase) applied to a conducing material, whether solid or fluid, will induce electric currents in the conductor, and hence a *Lorentz force* distribution: **Lorentz force**

$$\vec{f} = \vec{J} \times \vec{B} \tag{1.3}$$

where $\vec{f}[N/m^3]$ is the Lorentz's specific force, $\vec{J}[A/m^2]$ is the current density, and $\vec{B}[T]$ is the magnetic field.

This Lorentz force is in general rotational, and if the conductor is fluid, it is set in motion. Thus the magnetic field acts as a non-intrusive stirring device and it can, in principle, be engineered to provide any desired pattern of stirring. Forces may also be effected through the interaction of a steady current distribution driven through a fluid and the associated magnetic field.

When the field frequency is high, the Lorentz force is confined to a thin electromagnetic boundary layer, and the net effect of the magnetic field is to induce either a tangential velocity or a tangential stress just inside the boundary layer. The distribution of velocity or stress is related to the structure of the applied field. Symmetric configurations may lead to patterns of stirring in which the streamlines lie on toroidal surfaces; more generally, however, the streamline pattern is chaotic [93].

Lorentz's force can be applied in a different technical problem such as molten metals mixing: a contactless *electromagnetic stirring* is used in steels production, aluminum holding bath [26], silicon mono-crystal growth as in fig.1.1. **electromagnetic stirring**

Magnetic sources can be generated from a single phase system, 3-phase power supply (as a *translating magnetic filed* (TMF) [26, 17], a rotating magnetic field, or a twisted design [4, 5]) or a set of moving permanent magnets. The choice of the EM configuration affects the liquid behavior: in a single phase coil the average Lorentz's forces act radially as a pinch (fig.1.2(a)) splitting the liquid into two layers; a design with a 3-phase traveling magnetic field coils impose an upward average force as in fig.**??**.

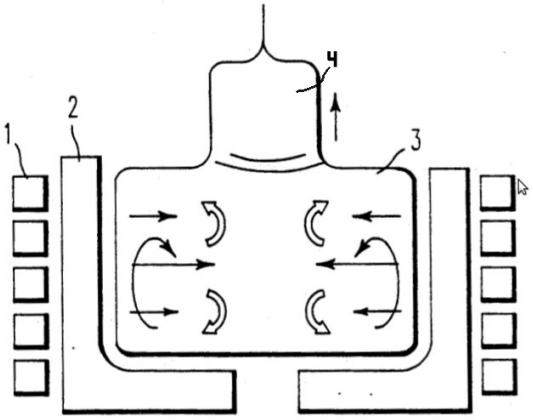

fig. 1.1: *Effect of induction stirring in a Czochralski pulling system (1) inductor coil, (2) graphite susceptor, (3) molten silicon, (4) pulled solid silicon mono-crystal [71].*

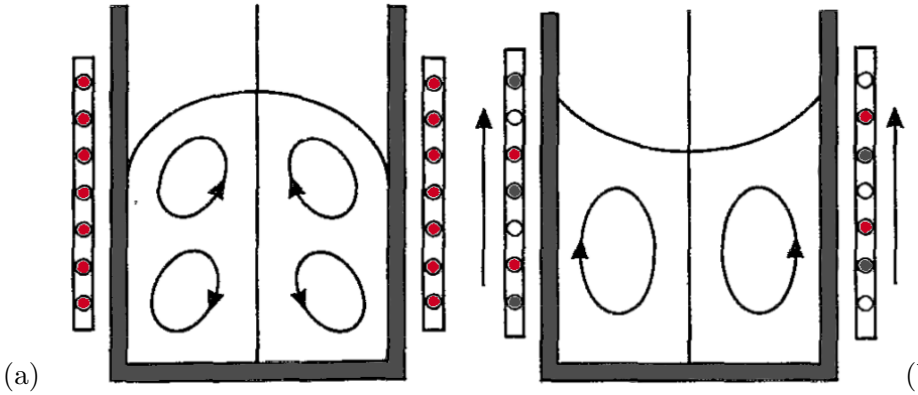

fig. 1.2: *Effect of different power supply over the fluid convection and free surface shape [93].*

EM pumps

The *EM pumps* design is based on the same principles [76, 124, 35].

The use of stirring equipment allows to:

- reduce process time and consequently energy consumption
- reduce melting loss
- improve metal quality by providing homogeneity in the chemical composition and temperature
- avoid moving parts for mixing (sometime otherwise impossible)

1.1.4 Magnetic dumping

Conductive liquid moving in a static magnetic field auto-induce a current density and hence a force opposing to the movement itself:

$$\vec{f} = \sigma(\vec{v} \times \vec{B}) \times \vec{B} \tag{1.4}$$

where $v[m/s]$ is the liquid velocity. This imply a suppression or reduction of flow. The *magnetic dumping* effect (or magnetic brake) is used in a lot of different situations in which the convective flow are to be avoided. Some industrial examples are in continuous casting, metal strip casting [109, 15, 90], and the Czochralski process.

magnetic dumping

In Czochralski growth of silicon crystals, the melt volumes and the corresponding crucible diameters were increased significantly in the last years (nowadays, crystals with a weight of more than 200kg are grown). The result is a *highly turbulent melt* during the growth with strong temperature fluctuations. These are detrimental during the seeding process because they cause strong variations of the diameter of the growing crystal in the necking phase that can cause severe mechanical problems if one takes into account the weight of the growing crystal hanging at the small diameter seed.

The uniformity of the diameter of the seed can be improved significantly due to the damping of the temperature fluctuations by using a steady magnetic field as a *magnetic brake* [64, 44, 80] (fig.1.3). Moreover the application of an horizontal magnetic field also influences the shape of the solid-liquid interface in a positive way reducing the surface curvature radius consequently obtaining the lateral uniformity of point defects which are an important quality criterion.

magnetic brake

1.1.5 Free surface and confinement of liquid conductive materials

Physically base on the same equations (eqs. 1.3 and 1.4) the Lorentz's force can be used to constrain liquid conductive materials defining the free surface. The *magnetic pressure*

magnetic pressure

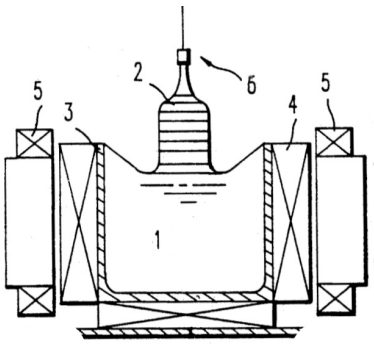

fig. 1.3: *Magnetic dumping in Czochralski pulling system used to freeze convective and superficial silicon movements and improve crystal quality. (1) molten silicon, (2) mono-crystal, (3) graphite susceptor/quartz crucible, (4) induction heating system, (5) DC magnetic brake circuit, (6) initial silicon seed [71, 64].*

$$p = \frac{B^2}{2 \cdot \mu_r \mu_0} \tag{1.5}$$

(where $p[Pa]$ is the pressure, $\mu_r[-]$ is the relative magnetic permeability, and μ_0 is the vacuum magnetic permeability) can arise from a gradient in permeability (material changes and interfaces) or in magnetic field disuniformity (induced currents, etc.). The understanding and modeling of free surface and interface is quite a complex problem involving moving boundaries, multi-phase systems, fluid instabilities and complex physical description [16]. Nevertheless, in engineering metals processing, the confining of a molten metal without use of mechanical equipment is of great interest. In cold crucible process or continuous casting, the control of a molten material ejection rate has strongly been desired for not only shaping the molten to particles with uniform size, but also precision coating of metals [7, 77].

levitation melting

Combining the heating effect, the surface control and the dumping effect a very promising perspective is in *levitation melting* systems [46, 16, 15, 72]. A cointainerless melting system allows to obtain high purity alloys in a controlled atmosphere.

float zone-method

A consolidated technology based on the control of the solid/liquid/gas interface is the *float zone-method* (FZ) as described in fig.1.4. Lot of computational and analytical studies are focusing on the design of a well-defined magnetic field configuration. The influence of the magnetic field for a contactless control and manipulation of the phase boundary and the segregation behavior during crystal growth is of crucial importance in the process improvement. Lots of investigation of the influence of the fluid flow on the

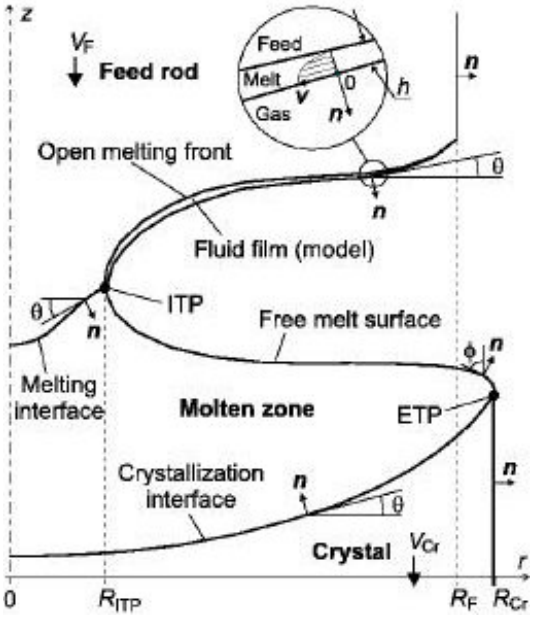

fig. 1.4: *Multi-physic regions and interactions to take into account during the simulation of a FZ process: solid/liquid, solidification and crystallization interface, free melt surface, melting zone, and fluid zone [105].*

dopant concentration and on the macro- and microscopic resistivity distribution in the crystal is performed [105].

1.1.6 Crystalline structure modification

Magnetic field's streamlines can define a preferred direction and interact with anisotropic materials or during solidification processes influencing or defining the growth of ordered structure in materials [132]. Ordered material structures can show innovative and interesting mechanical, electrical, chemical, and thermal properties [41, 42]. The *directional solidification* system is widely used to obtain large grains structure in semiconductors and ordered dendritic structure in metallic alloys.

directional solidification

MHD stirring can significantly modify the solidification structure. The effect of a permanent magnetic field on convection in directional solidification has been discussed. It has been determined that the application of a magnetic field during the directional solidification of materials can significantly reduce the thermosolutal buoyant flow. Most models of micro-structural formation neglect the influence of convection and only consider diffusional transport of either heat or mass away from the growing crystal. However, at

low growth rates, convection and its influence on micro-structure formation and development can become dominant and should not be neglected [82].

To fabricate crystal-orientated ceramics [7] a specimen is rotated during the slip casting under a high magnetic field. In substances with an anysotropic magnetic susceptibility in different axis, one-directional crystal orientation can be obtained (fig.1.5(a)).

(a) 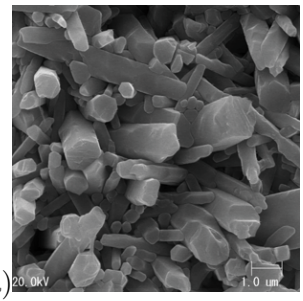 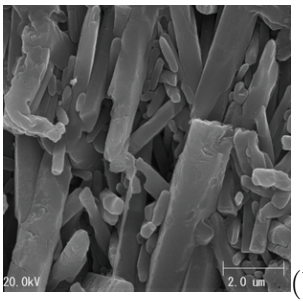 (b)

fig. 1.5: *SEM micrographs of specimens made of $\alpha - Si_3N_4$ (front and side view) [7].*

1.1.7 Skull-Melting Technologies

cold crucible

The induction *cold crucible* technology as one application of skull-melting is a well known method for melting and pouring of special alloys, such as titanium-aluminum, crystallize pure high temperature melting oxides (ZrO_2, Al_2O_3, etc.), conglobe nuclear wastes into vitreous structure without contamination, and others.

This method has unique characteristics:

- it can melt materials with high melting point [1]
- avoid any contamination from crucible walls
- create an homogeneous composition with strong stirring effect
- can be easily included in a controlled atmosphere system

[1] In order to melt non electrically conductive materials metallic inclusion (high temperature melting metallic rings, metal from which the oxide is made of, etc.) can be added in the initial phase to start the heating process [67].

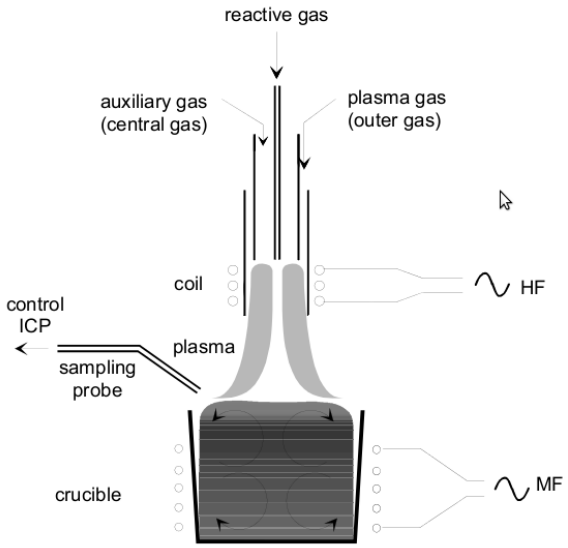

fig. 1.6: *Silicon plasma purification schema as in* PhotoSil *process with RF plasma coils and induction heating system in melt zone.*

Further improvement of the melting technology is necessary to widen the field of application in the direction of super-heating the melt in order to get better results for complex casting structures. Also, the combination of induction melting with plasma heating has to be investigated further in order to superheat the melt.

1.1.8 Plasma

It will be further discuss the application of *plasma* in the heating and refining of liquid silicon 3.1.1 as in fig.1.6. **plasma**

1.1.9 Laser processing of materials

In a wide range of technologies involving laser processing of materials, such as welding, surface treatment, drilling and cutting, a metallic melt is created. Applied magnetic fields, together with an electric current flowing through the melt, create volumetric forces modifying the pressure distribution, the flow field, and the heat transfer. This effect is used to modify the geometry and metallurgy of the re-solidified melt. In addition, a strong reduction of pore formation is expected owing to modified buoyancy force. In

drilling and cutting magnetic forces help to remove the melt. The interest is in numerical, experimental, and design studies to enhance significantly the quality and efficiency of laser processing of materials.

In the production of PV cells from silicon ribbon (see 3.1.2 at pag.44) lasers can be used to create a localize melting and recrystallization or to perform a rapid superficial thermal process [119].

1.1.10 Electrolytes

The goal is to increase knowledge about the effect of magnetic fields on electrochemical processes with the aim of producing ferromagnetic films, multilayers, and nanostructures (nanowires, nanopowders, etc.) with improved properties.

(a) 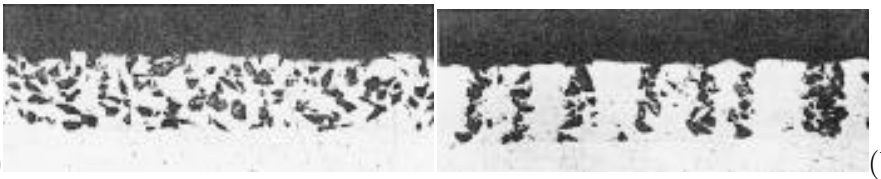 (b)

fig. 1.7: *Effect of magnetic field on $Ni\ Al_2O_3$ composite coating process (left with no field, right with $B = 7T$) [8].*

The action of the magnetic field on the bath properties manifests in the change of all the physical parameters. When a magnetic field is applied during an electrochemical process, the bath conductivity becomes anisotropic as a result of transverse concentration gradients of electrolytic species, which create an electric field in the direction perpendicular to the magnetic field.

Hall effect

This could be identified as *Hall effect*. In the same manner it has been observed that the diffusivity of the electro-active species, the viscosity, and the level of temperature of the bath are slightly modified.

Magnetic fields are used to control the mass transfer processes in the electrochemical cells [7]. In the most classical configuration the magnetic field is imposed perpendicular to the electrical current. In such a case the Lorenz force arises, and the *MHD* convection governs the hydrodynamic

boundary layers. When either paramagnetic or ferromagnetic species are involved, other forces exist that can affect the diffusion processes and the electrical conductivity of the bath. Some electrical phenomena have been neglected up to now. For example, for the non-equipotential electrodes, such as semiconductors, anisotropy effects could arise. All these magnetically induced convective effects can be used to control materials that are being deposited. The application of AC magnetic field could be used to solve specific problems for the improvement of mass transfer.

2

Simulation of the directional solidification of γTiAl alloys

Out of intense complexities
intense simplicities emerge.

Winston Churchill

Phase change is a very complex physical phenomenon that governs a lot of industrial applications. Due to the difficulties that arise in manufacturing, designing processes, in making observations of fluid flow inside molds because of very high temperatures and highly transient and risky conditions, **numerical modeling tools** are needed to predict the behavior of the different phases involved in metallurgical processes.

Therefore, **computational fluid dynamics** (*CFD*) is usually the most **CFD**

economical and practical way to get information about what is going on inside a casting device and it is often the only feasible way. Absorption or release of **latent heat** makes phase change problems **nonlinear** and exact solutions are only restricted to few problems involving pure substances in very simple domains. The inability of these solutions to address multidimensional effects, non-discrete or non-isothermal phase change, advection dominated situations, has moved the attention towards numerical procedures. Nowadays CFD packages are becoming well-suited tools to investigate all kind of transport phenomena, especially when **coupled fields** are involved. This trend has addressed the research in solidification problems towards the solution of models combining incompressible Navier-Stokes equations coupled with heat and mass transfer including phase change [100].

The formation of morphological features in solidification of pure materials and alloys has been investigated over many years. Solidification patterns is complex phenomena controlled by the interaction of thermodynamic, chemical, fluid-dynamics, and kinetics laws. Natural or forced convection on **micro-structure** results in morphologies that are potentially much different from those generated by purely diffusive heat and solute transport [10].

(a) 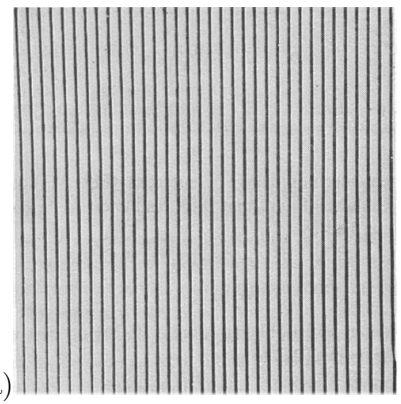 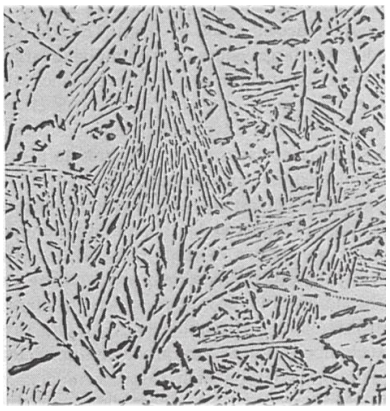 (b)

fig. 2.1: *Micrography of (a) directionally solidified binary alloy and (b) dendritic growth.*

Titanium and aluminum create a quite complex system of compounds described by the phase diagram in 2.2. In composition range 44-50 at% Al,

TiAl phase diagram presents a peritectic reaction which, in specific thermal and chemical conditions [116], leads to the growth of an **anisotropic lamellar metallurgical structure** [128].

In a wide range of applications, from automotive to power generation, this directional solidified $\gamma TiAl$ alloys has a strong interest arising from the specific properties that can be obtained (i.e. high mechanical strength, low density and corrosion resistance at high temperature) to replace nickel-based super-alloys as lightweight structural materials. Therefore, lamellar orientation control should be an important method to improve the performance of TiAl alloys [87, 86].

γ**TiAl**

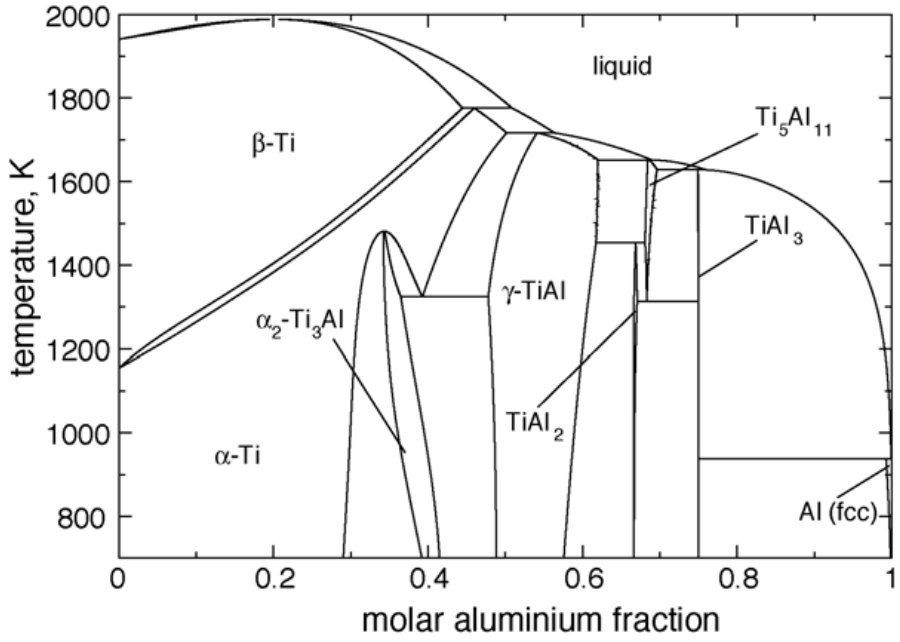

fig. 2.2: *Ti-Al Phase diagram [62].*

The possibility to design a casting process in order to obtain the best configuration possible can be based on the implementation of a **diretional solidification model** into a CFD package.

2.1 Phase Changes

In a phase diagram as sketched in fig.2.3 at each temperature T *Solidus*, *Liquidus* and phase lines describes the thermodynamically stable compounds.

In a multi-phase region[1], for a given composition C and temperature T, the *liquid fraction* f_L, *ie* the percentage of liquid over total volume or mass,

lever rule is given by the *lever rule*:

$$f_L(C,T) = \frac{C_s(T) - C}{C_s(T) - C_l(T)} \tag{2.1}$$

where C_s and C_l are the composition of the solid and liquid in thermodinamical equilibrium at that temperature.

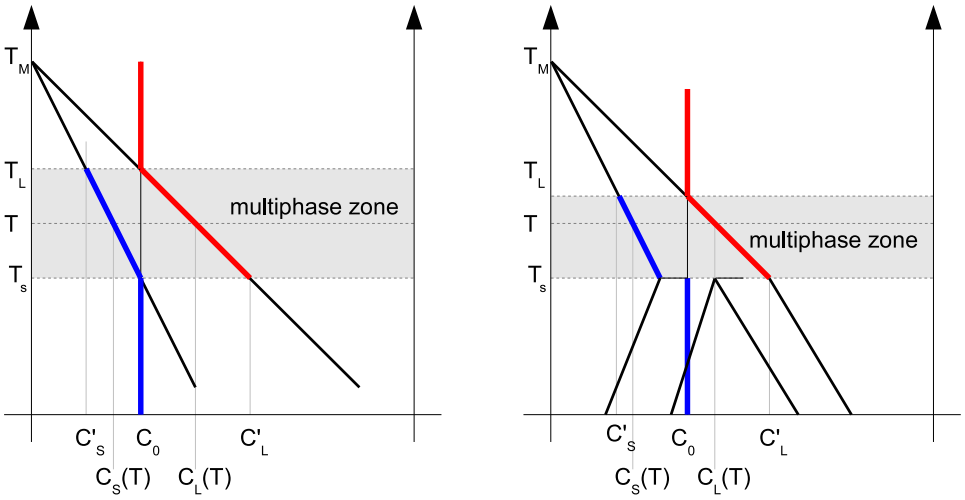

fig. 2.3: *Phase diagrams for a binary alloy (simple and peritectic)*

The number of independent variables (*degree of freedom*) needed to describe a state in a multi-physic and multi-component system can be easily

Gibbs phase rule found with the *Gibbs phase rule*:

$$DOF = N_{\text{components}} - N_{\text{phases}} + 2 \tag{2.2}$$

[1] A multi-phase region is a temperature/composition area in phase diagrams where two phases are mixed in a stable state without chemical reactions.

2.2 Stefan Condition

For any conservation law in the form [3]:

$$\frac{\partial A}{\partial t} + \nabla \cdot \vec{B} = f \tag{2.3}$$

where A is a scalar variable and $\vec{B}$ a vector field, the jump across a smooth surface can be shown to be:

$$\delta^{\pm}(A)v = \delta^{\pm}(\vec{B} \cdot \vec{n}) \tag{2.4}$$

where $\delta^{\pm}(x)$ is the difference between x values evaluated on surface sides, v is the surface normal velocity and $\vec{n}$ is the external unit normal vector. Applying eq.2.4 to energy conservation law, we find:

$$\delta^{\pm}(\rho C_p T)v = \delta^{\pm}(\vec{q} \cdot \vec{n}) \tag{2.5}$$

Since $\delta^{\pm}(\rho C_p T)$ represents the energy gap between liquid and solid it represents the latent heat. Thus, eq.2.5 becomes the *Stefan Condition*: **Stefan Condition**

$$\rho L v = \delta^{\pm}(\vec{q} \cdot \vec{n}) \tag{2.6}$$

For a mono dimensional solidification process the eq.2.6 becomes:

$$\rho L \frac{dx_{SL}}{dt} = -k_L \frac{\partial T}{\partial x}\bigg|_{x_{SL}}^{L} + k_S \frac{\partial T}{\partial x}\bigg|_{x_{SL}}^{S} \tag{2.7}$$

2.2.1 Stefan problem

The problem describes the melting process of a slab of length l from initial temperature T_i heated from one side with a fixed temperature source at T_{ext}, with imposed adiabatic condition all around and constant physical properties. The problem's equations are:

Partial Differential Equations:

$$\rho C_p \frac{\partial T}{\partial t} = \begin{cases} k_L T_{,xx} & 0 < x < x_{SL} \\ k_S T_{,xx} & x_{SL} < x < l \end{cases} \tag{2.8}$$

Initial Conditions: $t = 0$

$$x_{SL} = 0 \tag{2.9}$$

$$T(x) = T_i \quad 0 < x < l \tag{2.10}$$

Interface Conditions:

$$T(x_{SL}, t) = T_{melt} \quad \forall t > 0 \tag{2.11}$$

$$\rho L v = q(x_{SL}^-, t) - q(x_{SL}^+, t) \quad \forall t > 0 \tag{2.12}$$

Boundary Conditions:

$$T(x = 0, t) = T_{ext} \quad \forall t > 0 \tag{2.13}$$

$$-k_s \frac{\partial T}{\partial x}(x = l, t) = 0 \quad \forall t > 0 \tag{2.14}$$

Even if all characteristics are constant the *Stefan Problem* is a non linear **moving boundary problem**. This non-linearity arises from boundaries conditions set on points with unknown positions.

2.2.2 Explicit Solutions

Close-explicit solution of *Stefan Problem* can be found under very strict conditions:

- constant thermo-physical properties
- mono dimensional model
- semi-infinite geometry
- uniform initial temperature
- constant imposed temperature at the boundary

2.2.3 One-phase Stefan problem

Lets consider the melting process of a semi-infinite slab at the uniform initial temperature T_m with imposed temperature T_{ext} at the interface. In this specific problem the solid temperature is T_m constant in time and uniform for $x > x_{SL}$. The last condition set the only unknown parameters on liquid part.

Setting the solidification front position x_{SL} to be:

$$x_{SL} \propto \sqrt{t} \tag{2.15}$$

the solution of the one-phase Stefan problem is:

$$T(x,t) = T_L - \Delta T_L \frac{\mathrm{erf}(x/2\sqrt{\alpha_L t})}{\mathrm{erf}(\lambda)} \tag{2.16}$$

where

$$\Delta T_L = T_L - T_m \tag{2.17}$$

$$\alpha_L = k_l/\rho C_l \tag{2.18}$$

and λ is the root of the transcendental equation:

$$\lambda \exp(\lambda^2)\mathrm{erf}(\lambda) = St_L/\sqrt{\pi} \tag{2.19}$$

In phase change problem the *Stefan number St* **Stefan number**

$$St = \frac{C_L \Delta T_L}{L} \tag{2.20}$$

represents the sensible heat – latent heat ratio. Processes with large St can be solved just with pure conduction equation. For small St conduction heat transfer will be dominated by phase change.

Analytical solution

Simulated a 10cm TiAl slab at initial uniform temperature $T_s = T_m = 1500°C$ and heated from left side at constant temperature $T_l = 1550°C$. In this approximation temperature in the solid part is constant thus can be considered as a boundary condition for liquid calculation. Results are plotted in fig.2.4

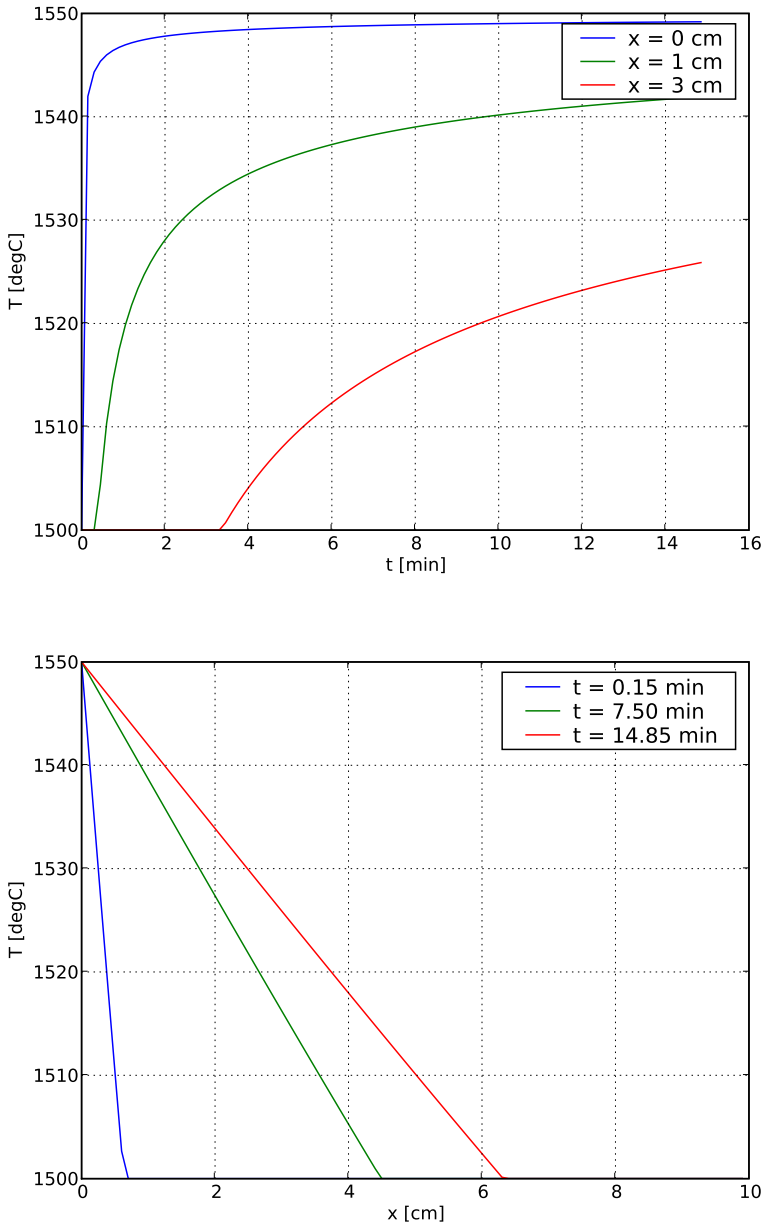

fig. 2.4: *Temperature from one-phase melting problem.*

2.2.4 Two-phase Stefan problem

The results of a simulated a 10cm TiAl slab at initial uniform temperature $T_s = 1450°\text{C}$ and heated from left side at constant temperature $T_l = 1550°\text{C}$ are shown in fig.2.5.

2.3 Numerical simulation for solidification process

The common approaches to solve a solidification problem are to ignore either conduction or diffusion uncoupling the physical problem. The former one considers a isothermal "thermodynamically stable" solidification process. The latter approach assumes constant composition in solid and liquid phases.

2.3.1 Simulations with mushy zone

The theory of the **quasiequilibrium two-phase** (mushy) **layer** is based on the assumption that the nascent supercooling is instantaneously reduced by growing dendrites and that there forms some **structureless two-phase zone**, separating the crystal and melt. The morphological instability of the phase interface and the instability of the metastable constitutionally supercooled binary solution (melt) cause a system of elements of the solid phase in the form of dendrites, columnar and uniaxial crystals to appear in the liquid phase. The development of this system reduces the supercooling and leads to formation of a new stable solidification mode characterized by the presence of a mushy layer that separates the crystal and the solution [2].

In this mushy transition zone between solid and liquid, the material properties are blended proportionally to the f_L (thermal conductivity and specific heat) [3]:

$$\lambda_m = f_L\lambda_l + (1 - f_L)\lambda_s \tag{2.21}$$

$$c_m = f_L c_l + (1 - f_L)c_s \tag{2.22}$$

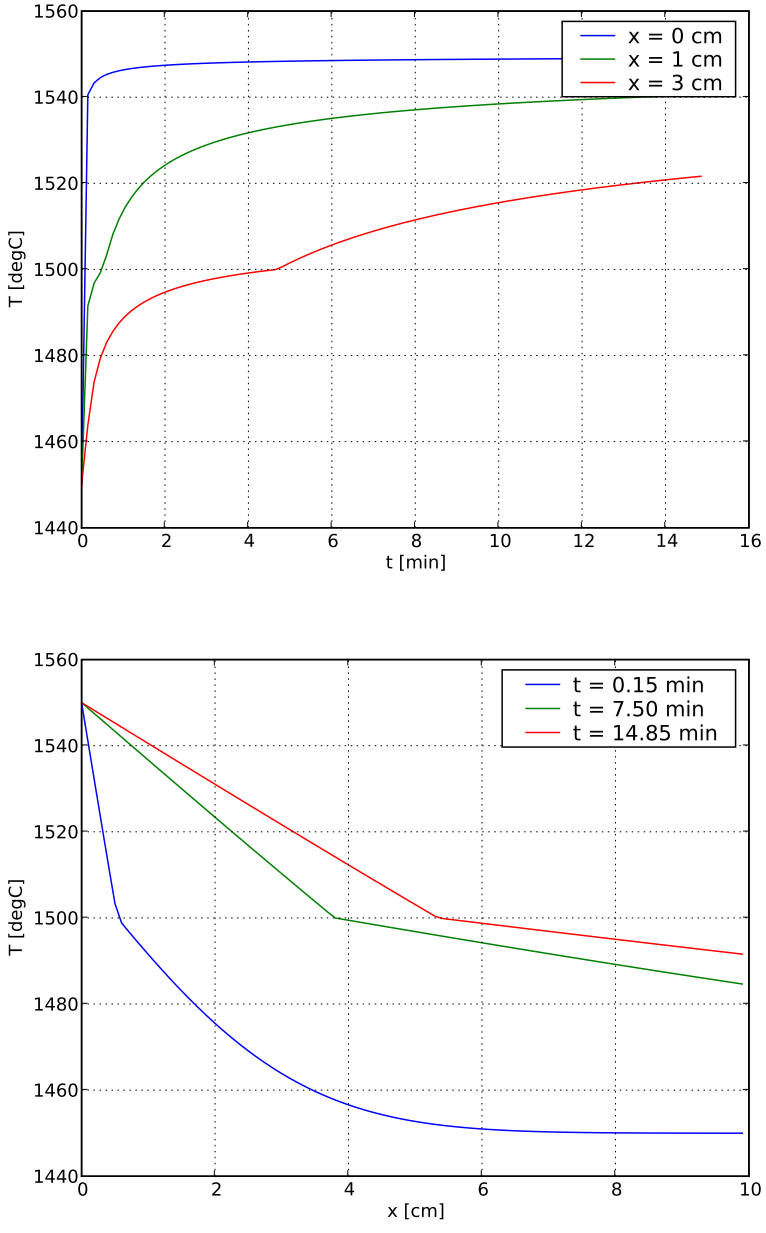

fig. 2.5: *Temperature from two-phase melting problem.*

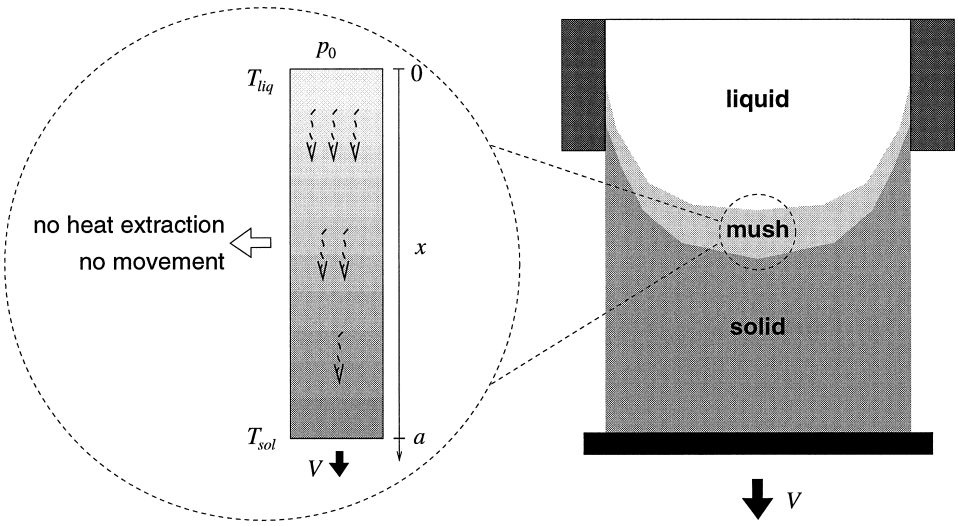

fig. 2.6: *Schematic representation of the mushy zone [52].*

2.4 Simulation with *Fluent*

The main goal of the numerical analysis is the better understanding of the parameters that affect solidification, the formation of the mushy zone and its effect on the micro-structure of materials. With this purpose, an investigation over the Fluent capabilities has been performed in order to evaluate the possibility to simulate the γTiAl directional solidification.

In the Fluent implemented solidification module there is no possibilities to modify phase change temperatures nor liquid fraction definitions via *User Defined Function* (UDF) [66] and those features are fundamental in the peritectic simulation.

For that reason, a new full solidification subroutine has been implemented. Liquid fraction (L_f) represents the local percentage of molten material volume. Fluent solidification module implements a simple linear L_f definition between the melting and the solidification points. The liquid fraction definition has been redefined in order to consider the peritectic

transformation:

$$L_f = \begin{cases} 0 & T < T_s \\ \frac{k}{k-1}\frac{T-T_s}{T-Tm} & T_s < T < T_m \\ 1 & T > Ts \end{cases} \tag{2.23}$$

where $T_s = \max(T_P, T_M + m_S C_0)$, C_0 is the alloy composition, $k = m_L/m_S$, m_L and m_S are the liquidus and solidus curves slope. The multiphase transition zone (mushy zone) affects both the thermal and the fluid-dynamic behavior. In this first steps the analysis is just on the influence on the thermodynamic part. The material properties has been updated using the new f_L definition: phase change temperatures are already implemented into the f_L definition itself and the thermal conductivity has been re-defined as:

$$\lambda(T) = \lambda_L(T)L_f + \lambda_S(T)(1 - L_f) \tag{2.24}$$

where λ_L and λ_S are the liquid and solid thermal conductivity (with temperature dependencies). There is no possibility to modify material specific heat C_p via UDF so a simple temperature interpolation has been set using the Fluent material data properties. The thermal diffusion equation has to be modified in order to consider the phase change:

$$\rho C_p \frac{dT}{dt} = \lambda T + (w_e + w_p) \tag{2.25}$$

where ρ is the material density, w_e is the sum of external specific power sources and w_p is the specific power released during solidification or required during melting process:

$$w_e = -\rho L \frac{dL_f}{dt} \tag{2.26}$$

where L is the fusion latent heat [3].

To validate the results, a simple comparison has been performed setting the new UDF to behave like the linear Fluent module. The model represents a cylinder of molten metal cooled from one side. In this first simulation the alloy has a non peritectic composition and the thermal conductivity is linear (see fig.2.7). Using the full non-linear UDF with the same model, setting a ipo-peritectic composition and a non-linear dependency of thermal conductivity the results differ (see fig.2.8) [24].

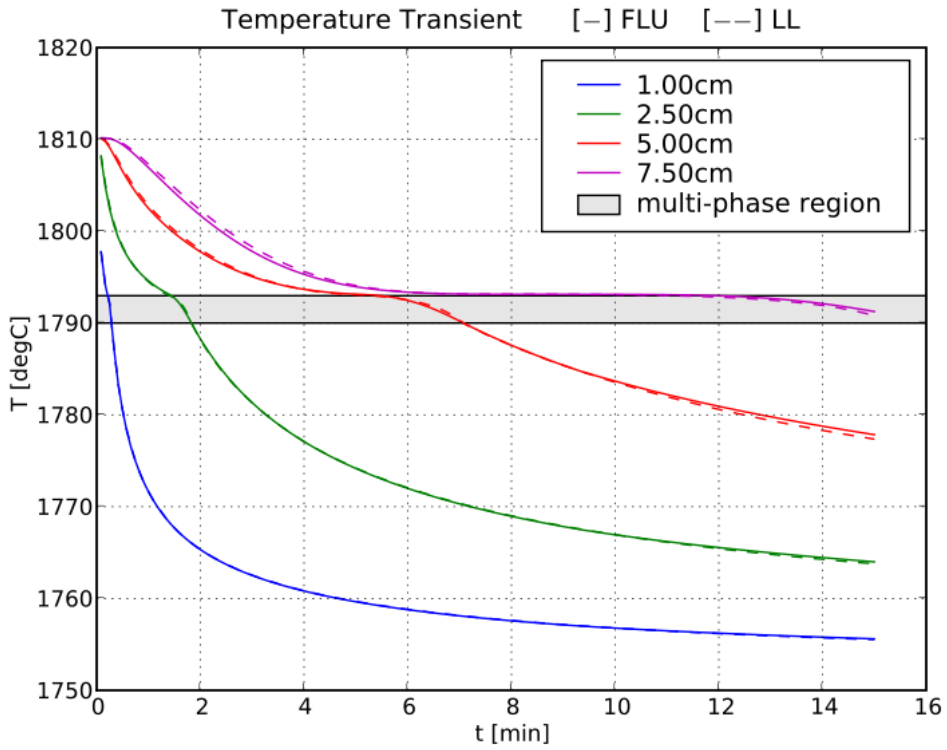

fig. 2.7: *Fluent results with the standard [-] and the new UDF [- -] using the same linear settings (non peritectic composition, linear thermal conductivity).*

Next steps in the UDF implementation will be the introduction of a smoothing function in the latent heat calculation in order to reduce simulation time (small time steps are currently required in order to manage the strong non-linearities connected with the peritectic behavior) and the introduction of the fluid-dynamic modification. The latter change requires the re-definition of the viscosity to take into account the phase and the mushy-zone characteristics:

$$\eta(T, L_f) = \eta(T)\frac{(1 - L_f)^2}{L_f^3 + \epsilon} \tag{2.27}$$

where η is the material viscosity and ϵ a predefined small number.

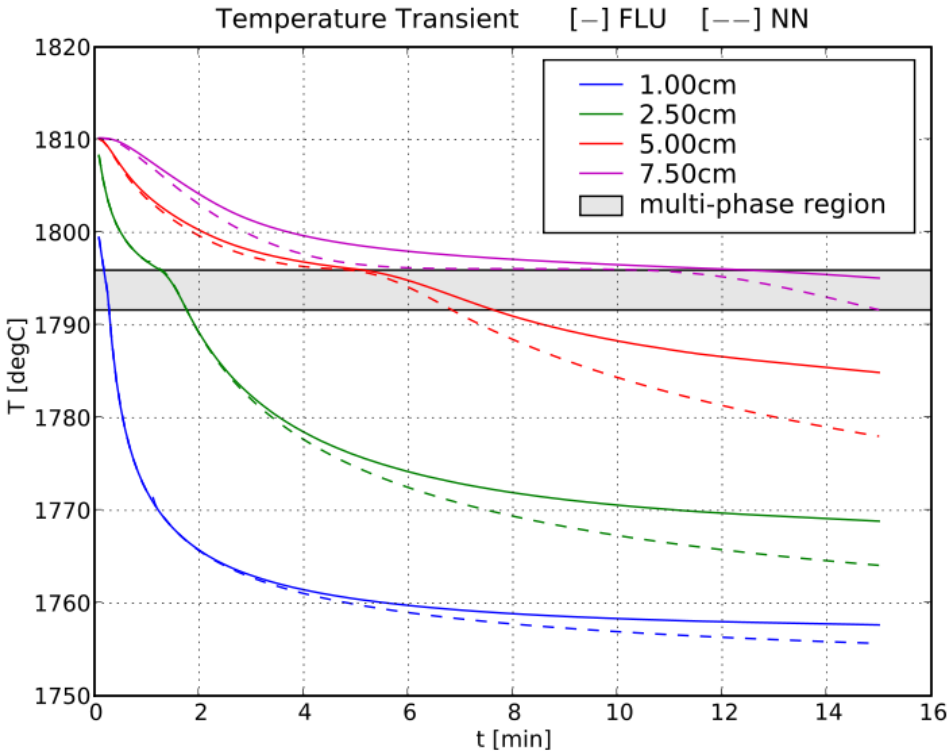

fig. 2.8: *Fluent results with the standard [-] and the new UDF [- -] using a peritectic composition and the non-linear thermal conductivity definition.*

3

Crystalline Silicon Production

The thing that hath been, it is that which shall be;
and that which is done is that which shall be done:
and there is no new thing under the sun.

Qoheleth

In the recent decades there has been growing interest in silicon material. It has been used for many years in the iron and steel industry for the production of iron-silicon alloys and, above all, for the production of lightweight alloys. For these latter applications, material with 99.8% purity level, called *metallurgical grade silicon* (*MG-Si*), are used and thus a complete production chain has been created. At the same time, silicon is the base of various products with applications from adhesive and sealant up to toothpaste. Nevertheless the most advanced technological applications are

MG-Si

those regarding electronics and solar technology [106].

Since the early 50s of the 20th century **semiconductors** become a world global need. Microelectronic components development required silicon of higher and higher purity and an increased feedstock production: new technologies for better quality and purification process had been developed to satisfy the spreading market requests. Considering the enormous importance of electronics in the current technology, industry, and life, crystal silicon is one of the most important technical materials today and, at least, in the near future [135].

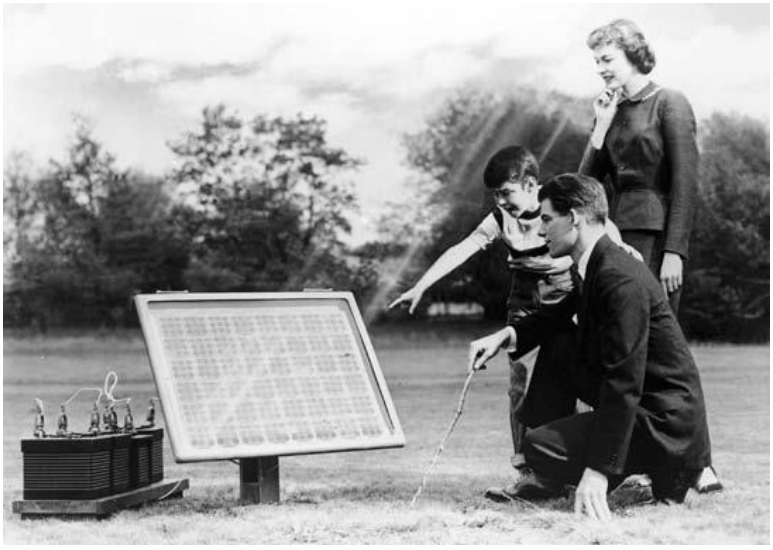

fig. 3.1: *One of the first advertisement on "Look Magazine" in 1956 about the PV technology developed by Bell Laboratories [103]*

alternative energy

The oil crisis in the 70s focused the world attention to find *alternative energy* sources other than oil or hydrocarbon. Public financial investments and scientific efforts on researches and technological applications led to develop PV market from small research components to the world everyday energy needs. In the frame of the "*20/20 program*" European governments are investing on alternative energy sources and, among them, PV seems to be the most promising technology for future small local production [51].

Several different technologies have been developed in PV area but the

world leading one is still based on **silicon** (amorphous, dendritic, poly- and mono-crystalline). High efficiency, low time degradation, a relatively low cost and non-toxic (compared to alternative compounds as Cadmium, Tellurium, Indium, Gallium, etc.), and its processing can be carried out without any particular risks to the environment in the most modern factories: those are the silicon success keys.

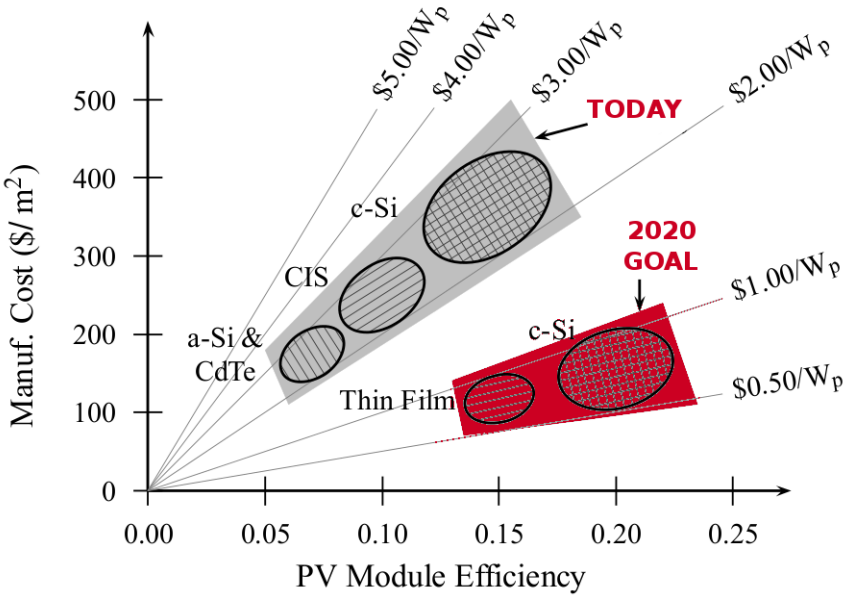

fig. 3.2: *Modules efficiency vs cost: today and future target [107].*

At present, about 95% of solar cells are made of silicon[1] (60% of those cells use *pSi* [106], 30% *mSi* and 10% of ribbon and thin-films) and 25% of the final modules cost is in feedstock (see fig..5.1 at pag.64) [111, 115].

In former time the main PV silicon source was in waste or rejected material from electronic crystal growth (tops and tails of mono rods, off-specification due to defects or oxygen content, broken wafers, pot scraps from CZ, etc.). The reduction in electronic *mSi* wasting due to processes optimization and the growth of the PV industry has been so rapid that

[1]The remaining 5% use combinations of Cadmium, Tellurium, Indium, Gallium, Selenium, etc. This percentage estimation is valid just for terrestrial "standard" solar cells. In PV concentration or spatial systems higher efficiencies in smaller surfaces are required [104]

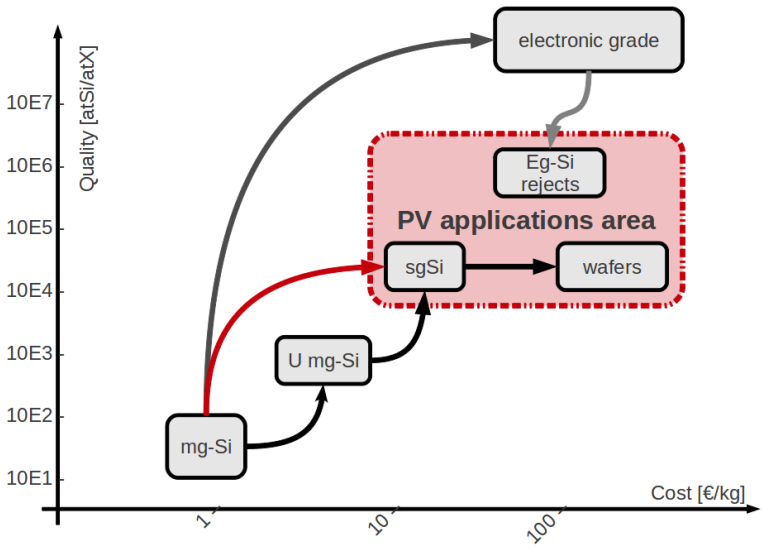

fig. 3.3: *Silicon grades costs and PV area [111, 9].*

in the period 2006–2008, there was a serious **shortage in the supply** of silicon feedstock used in the manufacture of PV cells [129, 69].

There is a clear gap both in price and purity between *MG-Si* and *EG-Si* (see tab.3.1 at pag.35), for this reason, worldwide research efforts were spent to fill this gap and define new ways to obtain *SG-Si* [104, 129, 39, 60]. The research trends can be summarized into three main concurring directions based on the study of:

- a low-cost processes for the production of *mSi* or *pSi* **wafers** and **ribbons**, alternative to the Czochralski process for the growth of crystalline silicon ingots [96, 9],
- a low-cost processes for the production of ***pSi* feedstock** using the gas phase route [43, 123], and
- the effects of combinations and limit of impurities and dopant acceptable in *SG-Si* adapted to solar cell fabrication, without loosing conversion efficiency and techniques [65, 9, 33, 32, 83].

The solution of problems associated to the production of a low grade silicon using variants of the *MG-Si* process looks very complex: the aim

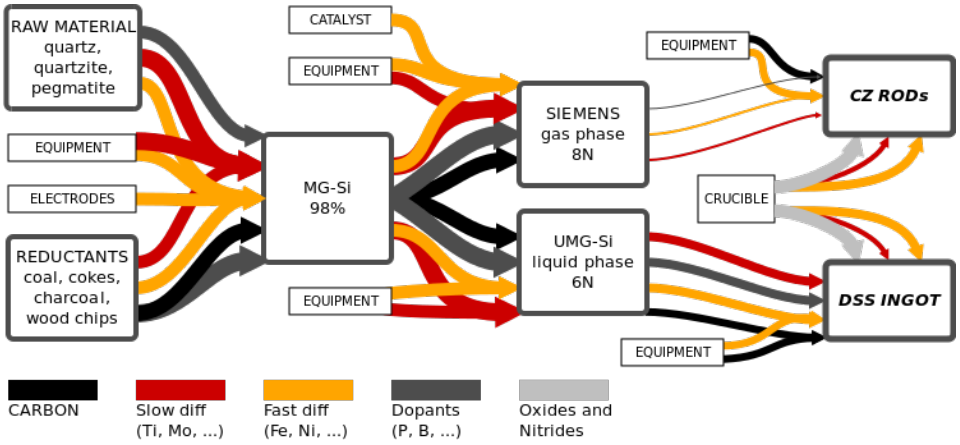

fig. 3.4: *Impurities sources and refinement process [34].*

to find *alternative routes* for the production of a low cost, low energy intensive polycrystalline feedstock is very hard because any material based on this processes would contain a quite large amount of **impurities** and **structural defects** (fig.3.4). Therefore, intense basic research studies were spent worldwide, with the objective of investigating the role of impurities (see fig.3.4) and crystal defects on the minority carrier lifetime and minority and majority carriers mobility and to discover/develop remedies in their presence [9, 83, 37].

alternative routes

3.1 Silicon production for PV applications

Silicon is the second most abundant element into the earth crust. Pure silicon crystals are only occasionally found as inclusions with gold and in volcanic exhalations [54, 55]. In nature it can be found as silicon dioxide (SiO_2 aka silica or quartz) or in combination with a lot of other different impurities or elements (Mg, Al, etc.).

3.1.1 Silicon grades

Even though is quite easy to find "good" quality SiO_2, the process to produce silicon is quite complex and energetically expensive (fig.3.5). The

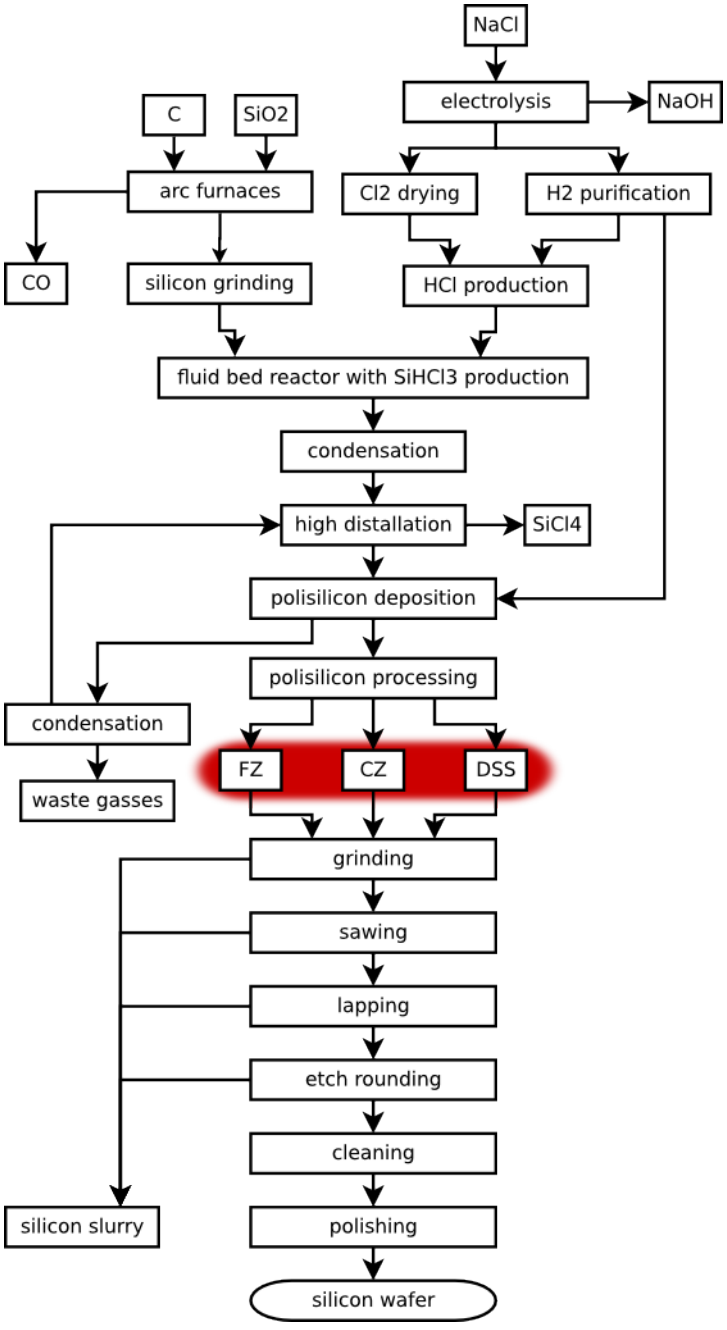

fig. 3.5: *Wafers production chain from SiO_2 to wafers.*

main pure silicon target is the electronic market and this common feedstock limited in former time the initial PV silicon market development.

Most of the electronic devices must be made from dislocation-free mono-

impurities	***MG-Si***	***UMG-Si***	***SG-Si***	***EG-Si***
B	40	<30	<1	<0.0001
P	20	<15	<5	<0.0003
O	3000	<2000	<10	<0.1
C	600	<250	<10	<0.1
Fe	2000	<150	<10	<0.001
Al	100 - 200	<50	<2	-
Ti	200	<5	<1	<0.003
Cr	50	<15	<1	<0.000001

Table 3.1: *Target impurities concentration in ppm_w for MG-Si, SG-Si and EG-Si [111, 113, 65].*

crystalline silicon of high crystalline perfection and homogeneity. Hence the *MG-Si* has to be purified before any semiconductor can be made reducing the total elements concentration other than carbon and oxygen to below 1*ppba* [135] (fig.3.3). To be qualified as **Electronic grade** (*EG-Si*) silicon has to be at least *8N* (*ie* 99.99999999%) or higher. Due to larger devices size and fewer restrictions PV silicon has just to be at least a *6N*.

Metallurgical grade

MG-Si

Metallurgical grade silicon (*MG-Si*) is the precursor for solar-grade and electronic-grade. Silicon is commercially prepared by the reduction at 2400K of high-purity silica (SiO_2) with wood, charcoal and coal in an electric arc furnace with graphite electrodes as in fig.3.6.

$$SiO_2 + 2C \rightarrow Si + 2CO \tag{3.1}$$

Molten silicon collects in the bottom of the furnace and it is drained out, casted and cooled. The *MG-Si* produced via this process is at least 98% pure. The element contamination can be in metals as aluminum, vanadium, boron, and phosphorus as well as inclusions of silicon carbide, silicon nitride, silicon dioxide, and others.

In 2005 *MG-Si* production is 900000 tons/year, of which 50% was for

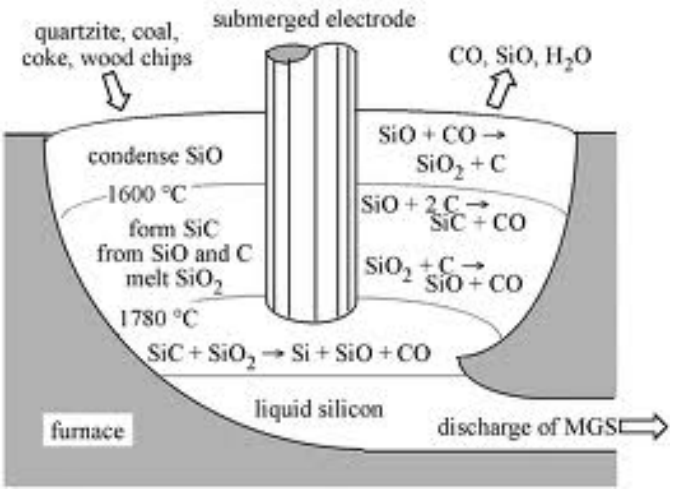

fig. 3.6: *Arc furnace schema and chemical reactions in the production of MG-Si [54, 28].*

production of aluminum, steel and titanium. About 45% was for the production of silicone and just the 5% used for the production of semiconductors (electronic and PV).

The purity of the *MG-Si* obtained is highly dependent on the quality of the initial raw material. If the initial sand quality is very high the silicon is finished off using chemical reactants reaching the *UMG-Si* (*upgraded metallurgical grade silicon*). To reach higher quality there are other ways to refine the silicon: the *chemical* and the *physical* purification [106, 18].

UMG-Si

Chemical route

chemical processes

The *chemical processes* are based on the fractional distillation of silicon compounds as tri-chloro-silane *TCS* ($HSiCl_3$), silane (SiH_4) and silicon tetrachloride ($SiCl_4$)[2]. All those compounds, obtained via chemical reaction between silicon and hydrochloric acid, are toxic, corrosive, irritating and explosive [122, 9, 18].

In **Siemens process** the decomposition of a very pure TCS gas take

[2]The *fractional distillation* process is based on the differences in boiling points in a liquid mixture. For instance the poiling points at atmosferic pressure for SiH_4 is -112.3°C and for $SiCl_4$ is 57.6°C [113]. Other compounds from non silicon reaction, as $AlCl_3$, $FeCl_3$, PCl_3, and so on, can be distilled this way.

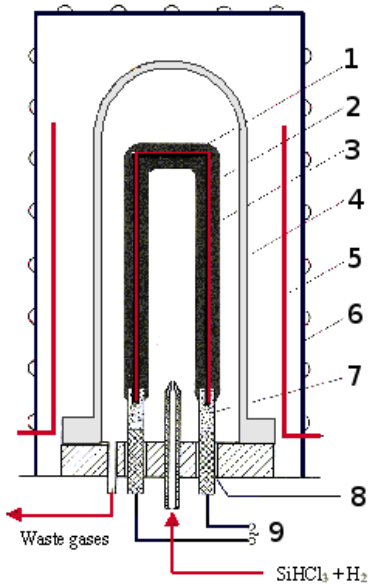

fig. 3.7: *Poly-Silicon reactor schema: (1) silicon bridge, (2) silicon core, (3) deposited pSi, (4) quartz bell jar, (5) pre-heater, (6) water-cooled thermal schield, (7) graphite, (8) thermal insulation, (9) electric power supply.*

place in special reactors over pure silicon heated rods (see fig.3.7) at 1150°C.

$$4HSiCl_{3(g)} \rightarrow Si_{(s)} + 2H_{2(g)} + 3SiCl_{4(g)} \tag{3.2}$$

Similar decomposition can be performed on pure silicon seed granules sustained by hot reactive gasses in a *fluidized bed* reactor (see fig.3.8). This process offers some significant advantage compared to the Siemens process as energy consumption and continuous production capability. The granulated *pSi* obtained can be used in continuous feeding process or to refill batch process [129, 122]. **fluidized bed**

All those chemical processes can give an extremely high purity silicon but are energetically expensive and requires a globally complex production plant.

Physical route

To reach higher purity of chemically purified silicon or to make a better silicon from *UMG-Si* a *physical purification* process can be used. Solid silicon shows a very low solubility for most of the elements, much lower than liquid silicon, resulting in a strong segregation of these elements in **physical purification**

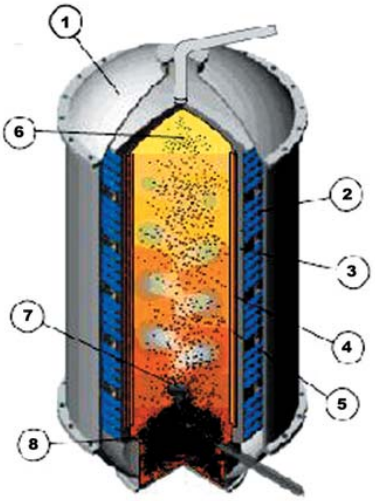

fig. 3.8: *Fluidized bed reactor for silicon purification. (1) chamber, (2) induction coils, (3) insulation, (4) susceptor, (5) liner, (6) silicon seeds, (7) silane feed, (8) pSi granules [55].*

freezing. Consequently the most of impurities remain dissolved in the melt and the final distribution follows the Scheil's equation (fig.3.9(a)):

$$C_f = kC_0(1-f)^{k-1} \tag{3.3}$$

where k is the distribution coefficient, f is the solid fraction (solidified mass over total mass), C_0 is the initial impurities concentration, C_f is the impurities concentration at the liquid/solid interface[3]. If the solidification process is performed "directionally" the last solidified part would be rich in impurities leaving a better purified middle zone. In particular Czochralski (CZ), Float Zone (FZ), and Directional Solidification System (DSS) processes are based on physical purification.

Plasma Purification

plasma torch

A solution to the problem of the shortage of silicon feedstock used to grow multi-crystalline ingots can be the production of a feedstock obtained by the direct purification of *UMG-Si* by means of a *plasma torch*. In fig.3.10 the standard process and the *PhotoSil* process are compared. Lot of studies (see [38, 56, 78, 131, 1, 49, 108, 114, 130, 48, 121]) are focused on this

[3]Iron has a distribution coefficient $k = 6.410^{-6}$. This means that from 150.000 iron atoms in the melt at the freezing interface only one iron atom is incorporated into the growing solid crystal.

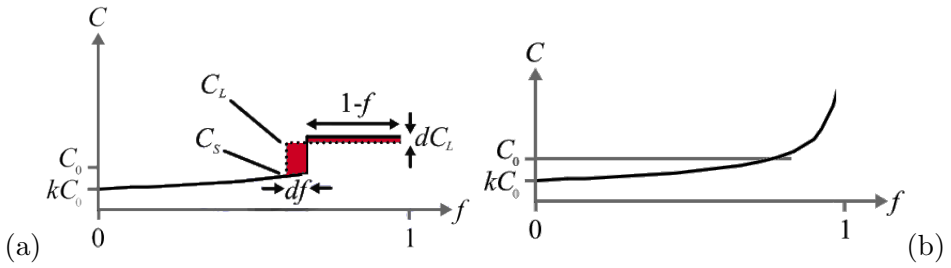

fig. 3.9: *Distribution of composition (impurities) during the solidification process and the Scheil equation derivation.*

purification process inorder to validate and optimize the efficiency and the removal of the larger ammount of impurities.

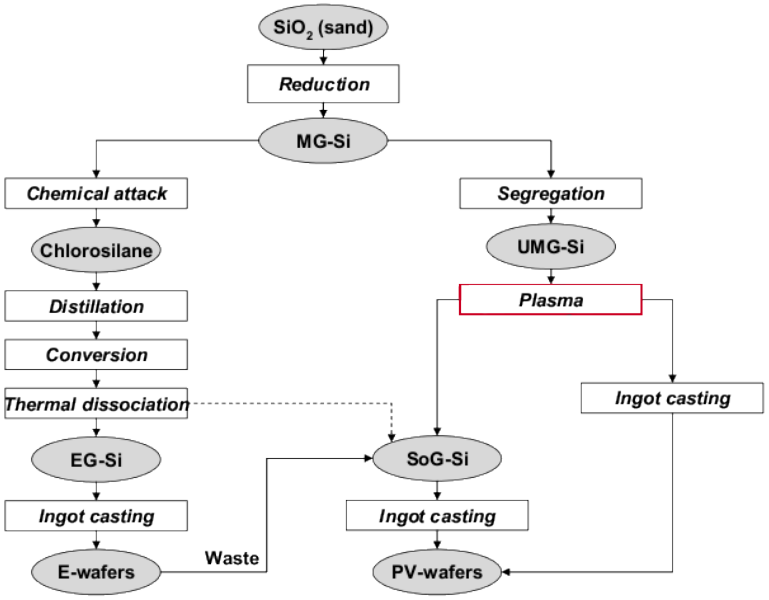

fig. 3.10: *Comparison between standard chemical route (left) and plasma purification* PhotoSil *process (right) [121].*

3.1.2 Silicon crystallization

The *pSi* obtained via the chemical route or *MG-Si* can not be used in any semiconductor application: the best performance can be achieved just increasing the crystals sizes in order to avoid defects mainly located in

grain borders. A single almost perfect crystal has to be used in electronics applications. Alternatively PV silicon can be produced in thin amorphous ribbons or deposited as layers on transparent glasses [94].

Single crystal silicon

Silicon wafers made from mono-crystalline silicon have the highest efficiency of conversion of solar energy into electricity (up to 25%).

The Czochralski process (CZ) is a method to produce single crystals from a liquid bath by introducing a pure crystal seed and slowly pulling upwards while rotating (fig.3.11). Crystal size and characteristics are defined by thermal gradient, rotation and pulling speed, and liquid purity. Nowadays, single silicon crystal rods can reach 450mm in diameter and 2m in length. For the growth of pure silicon crystals a quartz glass crucibles must

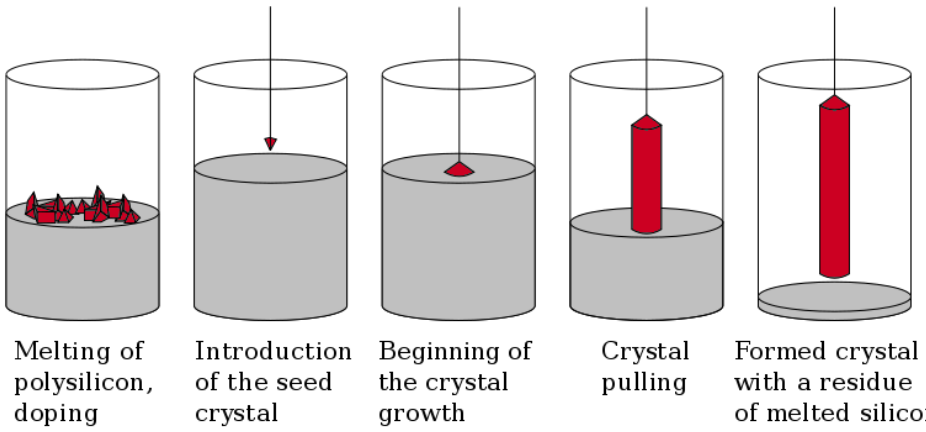

fig. 3.11: *Czochralski process schema.*

be used. Silicon reacts with crucible SiO_2 but oxygen can easily removed from melt as it strongly evaporate as gaseous SiO. The process chamber has to be strongly purged with inert gasses (argon, or helium) to remove quickly the silicon mono-oxide evaporating from the melt. Without purging a SiO and SiO_2 slug would form on the melt surface and the crystal growth would be impossible.

Float Zone process (*FZ*) completely remove the crucible contamination problem: a *pSi* rod of high grade is passed through an induction heating coil, which creates a localized molten zone from which the crystal ingot grows (fig.3.12). A seed mono-crystal is used at one end in order to start the growth. The whole process is carried out in an evacuated chamber or in an inert gas purge. As in the CZ process, the molten zone carries the impurities away with it and hence reduces impurity concentration.

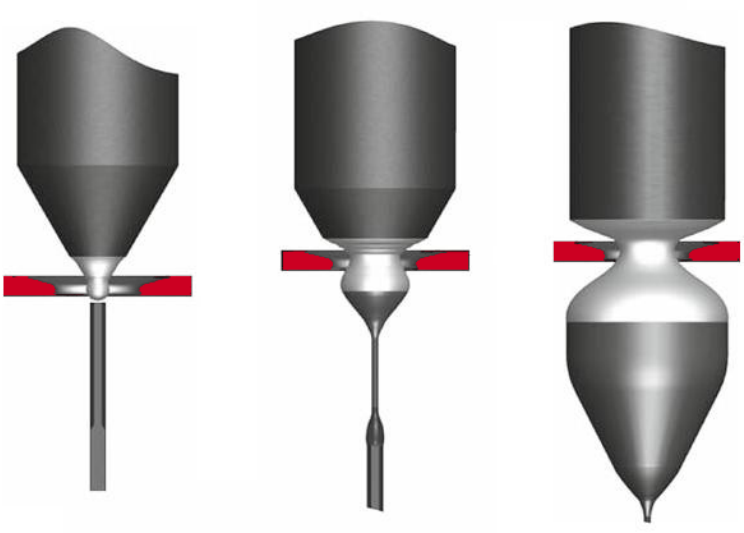

fig. 3.12: *Float Zone schema from initial seeding to growth.*

Multi-crystalline silicon

A multi-crystalline structure with grains on the order of mm to cm in width and approximately columnar along the solidification direction is the characteristic of the *directional solidification* (*DS*).

directional solidification

The Directional Solidification System (*DSS*) is going to be described in details in the next chapter but it is based on a quite simple design: the bottom side of a quartz crucible full of molten silicon is slowly cooled maintaining a **vertical thermal gradient**[4] by heating the upper zone.

[4]Sometime DSS is referred as "*vertical gradient freeze system*".

	CZ	FZ
growth speed [mm/min]	1 - 2	3 - 5
crucible	yes	no
consumables	crucible	none
heat-up / cool-down times	long	shot
Specific power consumption $[kWh/kg]$	30 - 60	30
axial resistivity uniformity	poor	good
Oxygen content $[ats/cm^3]$	more 10^{18}	less 10^{16}
Carbon content $[ats/cm^3]$	more 10^{17}	less 10^{16}
Metallic content	higher	lower
crystal diameter [mm]	150 - 200	100 - 150
operator skill	less	more
pSi feed form	any	crack-free rod

Table 3.2: *Comparison between Czochralski and Float zone processes [28]*

In the ideal configuration there should be almost no liquid convection and crystals would grow from bottom to top. Further consideration on the DSS design will be discussed later. DS can be carried out in a separate crucible after melting (liquid silicon is poured directly into the crucible, possibly re-heated and solidified) or directly melted and solidified in the same crucible.

The ElectroMagnetic Continuous Casting (*EMCC*) has some similarities to the casting and DS methods just described, but also has several unique features that change the ingot properties. EMC is based on induction-heated *cold-crucible* melt confinement, except that unlike the conventional cold crucible, there is no crucible bottom. A parallel, vertical array of close-spaced, but not touching, water-cooled, conducting copper fingers is attached at one end to a water-cooling manifold while the other end of each finger is closed. An internal distribution system carries cooling water to the tip and back again. The shape of the region enclosed by the close-spaced fingers determines the cross section of the cast ingot, and a wide variety of shapes are possible (circular, hexagonal, square, rectangular,

cold-crucible

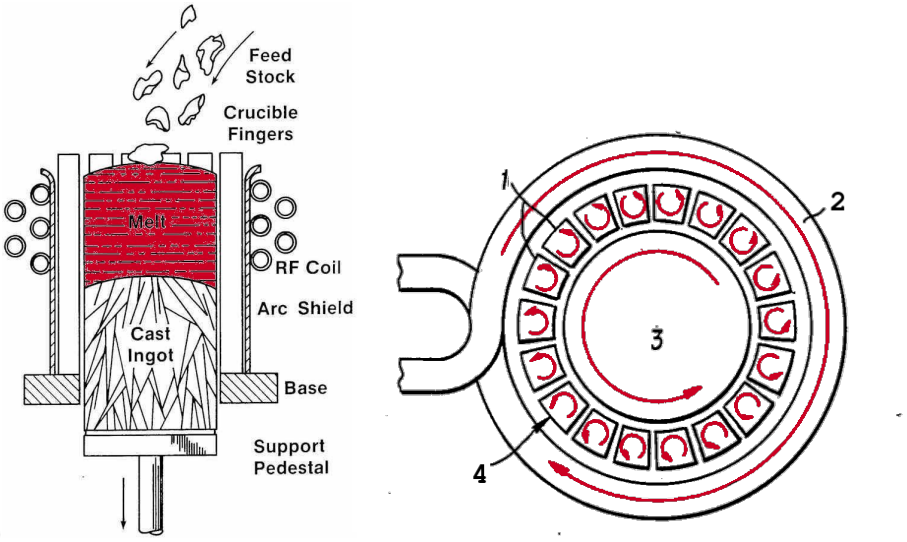

(a)

(b)

fig. 3.13: *EMCC schema and cold-crucible top-view explanation (1) finger, (2) external inductor and current direction, (3) induced current in melt, (4) current direction in fingers [28].*

etc.). Silicon is melted on a vertically movable platform (typically graphite) located within the finger array (fig.3.13(a)). The melting is accomplished by induction heating after suitable preheating. The induction coil, placed outside the finger array, induces a current to flow on the periphery of each finger, around the finger's vertical axis (fig.3.13(b)). Like a high-frequency transformer, each finger in turn induces a current to flow in the periphery of the silicon charge, about its vertical axis. The silicon is heated by Joule's effect. Furthermore electrodynamic repulsion between the current flowing in the periphery of the silicon melt and the currents flowing in the fingers. Thus, the melt is repulsed from the water-cooled fingers. The open-bottom arrangement allows the platform to be withdrawn downward, solidifying the molten silicon, while new melt is formed by introducing feed material from the top. In this way, a semi-continuous casting process can be carried out [28, 21, 68, 70, 98, 99, 47].

A variety of feed silicon geometries can be used (melts, rods, pellets, scrap, etc.). Because the interface is submerged, feed perturbations or slag

at the melt surface do not affect the solidification front. Ingot lengths of 10m have been demonstrated. The cross section of the ingots has evolved over years of development and is currently about 350 mm x 350 mm. The cold fingers allow steep thermal gradients and fast growth speeds (1.5-2.0 mm/min), even in ingots with large cross sections. Thus, grains are neither as columnar nor as large as in conventional DS.

Ribbon and sheet silicon

More than a dozen techniques have been introduced over the years for growing silicon ribbons or sheets. The main advantage of these processes is to avoid the kerf losses and obtain directly the wafer area to be treated.

Two methods developed commercially are the growth with edge supports, and the growth on a substrate. All these methods can be placed in two categories [94, 28, 122, 110, 109, 30, 31, 73, 118]

- those pulled **perpendicular** to a solid/liquid interface with the same shape as the ribbon cross section (web growth, capillary die growth, and edge-supported growth), and
- those pulled at a **large angle** to a solid/liquid interface that is much greater in area than the cross section of the sheet (growth on a substrate)

Edge-supported pulling of "string ribbons" uses a crystalline blade supported by two filaments as initial seed fig.3.14(a). A liquid silicon meniscus continuously feed the growing crystal ribbon. Thermal gradient, pulling speed and lot of other parameters influence the dislocation distribution and the final quality. The filaments are introduced through small holes in the bottom of either quartz or graphite crucibles. Ribbons as wide as 8cm have been grown, with the standard commercial size now being 5.6cm wide x 300mm thick. The ribbons are grown at about 1-2 cm/min pulling rates, giving a throughput of about $1m^2$/day. Furnaces can be kept in continuous

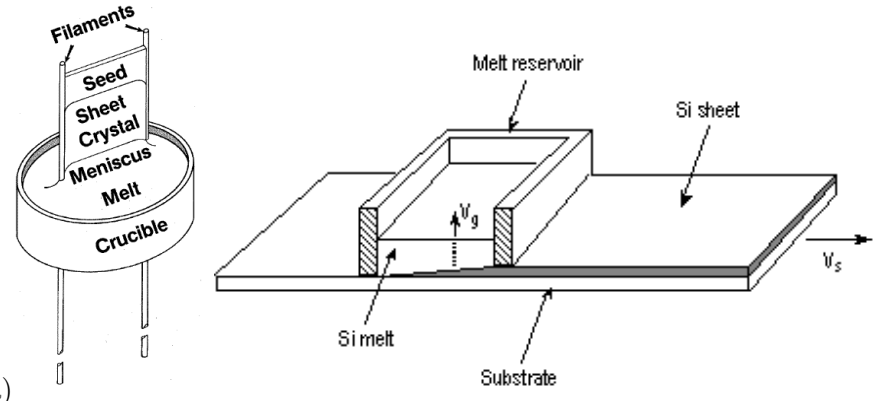

(a) (b)

fig. 3.14: *Growth with Edge Supports and Horizontal Growth on a Substrate.*

operation for weeks at a time by replenishing the melt. Ribbon sections of a desired length are removed by scribing while pulling is in progress. Continuous growth of more than 100m of ribbon has been achieved, and lengths greater than 300m have been obtained from a single furnace run (with successive seed starts). The steady-state grain structure contains longitudinal grains of about $1cm^2$ area, predominantly with coherent boundaries, in the central portion of the ribbons, and newly generated grains at the ribbon edges [28, 122].

Horizontal growth from the melt surface drown crystals horizontally from the free surface of melts. Many approaches have been considered for applying this process type to PV silicon. The ones currently under engineering development move a substrate through a hot zone tailored in such a way that a long region of molten silicon in contact with the upper surface of the substrate solidifies with a long wedge-shaped crystallization front as in fig.3.14(b). Coupled with moderate thermal gradient values (160°C), 250mm-thick sheets can then be grown with pulling speeds as high as 6 m/min. Heat removal is facilitated by the fact that the surface in which heat of crystallization is generated is nearly parallel to, and in close proximity to, the surface from which it is to be removed. The solid/liquid interface's growth direction is essentially perpendicular to the pulling direction so, as

grains nucleate at the substrate surface, their growth is columnar across the thickness of the sheet. This is in contrast to longitudinal grains aligned along the pulling direction obtained in the vertical techniques. The grains tend to be smaller in type II growth methods. Production solar cell efficiencies as high as 12% are attainable at the present time, and the best small-cell efficiency is 16%. The substrate does not have to remain with the grown sheet, and may be engineered for clean separation at some point after solidification.

3.1.3 Thin layer silicon

Thin-layer silicon is considered to be less than 50μm thick and deposited on a foreign substrate. Potential advantages of thin-layer approaches include less silicon usage, lower deposition temperatures relative to melt growth, monolithic module construction possibilities, and a tolerance for lower τ (the distance charge carriers have to travel is shorter). Disadvantages include incomplete light absorption and therefore the probable need for light-trapping, a likelihood that grain sizes will be small[5], and difficulty in making rear contacts if the substrate is an insulating material.

There is not yet any significant quantity of thin-layer crystalline silicon in commercial production for PV because only partial successes have been achieved in meeting the challenge [28].

[5]Grains recrystallization can be achieved by focused laser heating or electron beam [122].

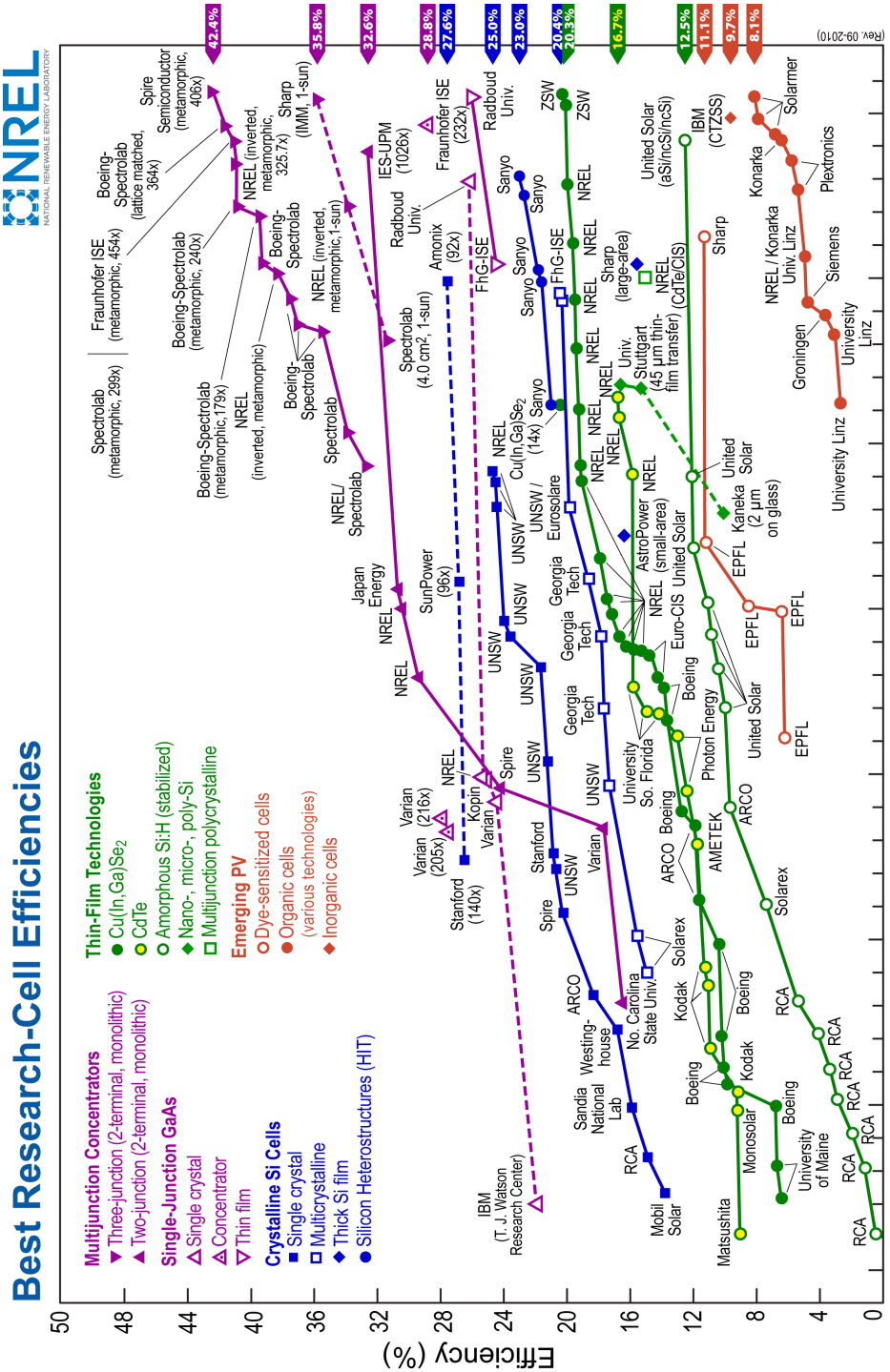

fig. 3.15: *NREL annual "best-efficiency" up to September 2010 [75].*

4

Directional Solidification System

There's a way to do it better find it.

Thomas Edison

The **Directional Solidification System** (*DSS*) used to produce *pSi* has a large share on the PV market because of the advantages in wider feedstock tolerance, lower manufacturing costs, higher throughput and simpler process and equipment compared to Czochralski or Float Zone processes [126]. Nevertheless the overall cost advantage of €/W still goes for *pSi*, the main detraction has been the lower efficiencies obtained with *pSi* compared to *mSi*, but process optimization is rapidly increasing conversion efficiency up to 20% (see fig.3.15). **DSS**

PV cells efficiency is related, among other, to defects in the crystalline

silicon structure and grain borders acts as a recombination center for the photogenerated carriers. In a multi-crystalline structure as in fig.4.1(a).1 carriers are trapped inside grains boundaries; conversely, in a columnar multi-crystalline structure as in fig.4.1(a).2 the path from the electron/gap creation area and the front/rear cell connections is almost free. The larger the grain sizes the higher would be the cell efficiency [122]. The ideal configuration in fig.4.1(b) is the base used to develop the nowadays widely used Directional Solidification Systems.

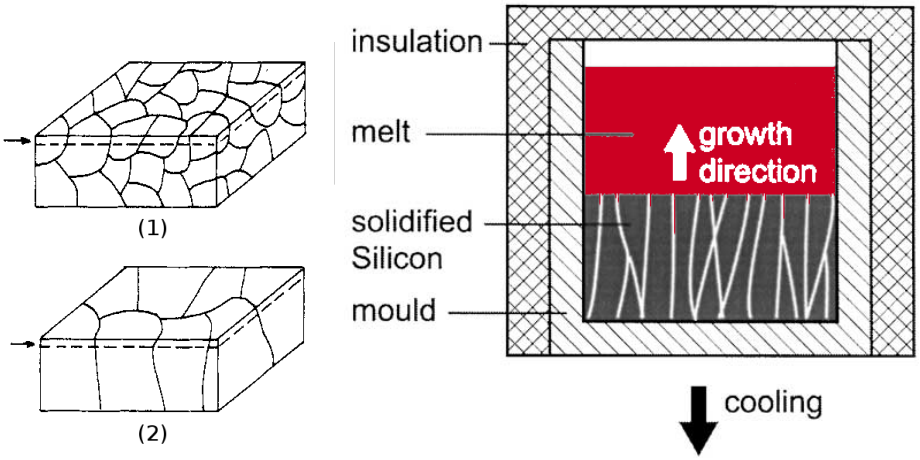

(a)

(b)

fig. 4.1: *Grain structure comparison for pSi with normal orientation (1) and directional solidification (2) and [left] DSS base concept [122].*

4.1 DSS process

A schematic of a DSS station with opened insulation is shown in fig.4.2. After the crucible with silicon charge is loaded in the station, the insulation is closed (fig.4.3(b)). The entire system is heated until the silicon charge is completely melted. To start silicon solidification and crystals growth, the insulation is moved (up or downward depending on the system design) while all the other components remain stationary (fig.4.3(c)). The bottom block will therefore lose heat to the cold environment primarily by radiation. This causes high heat extraction from the bottom of crucible, initiating

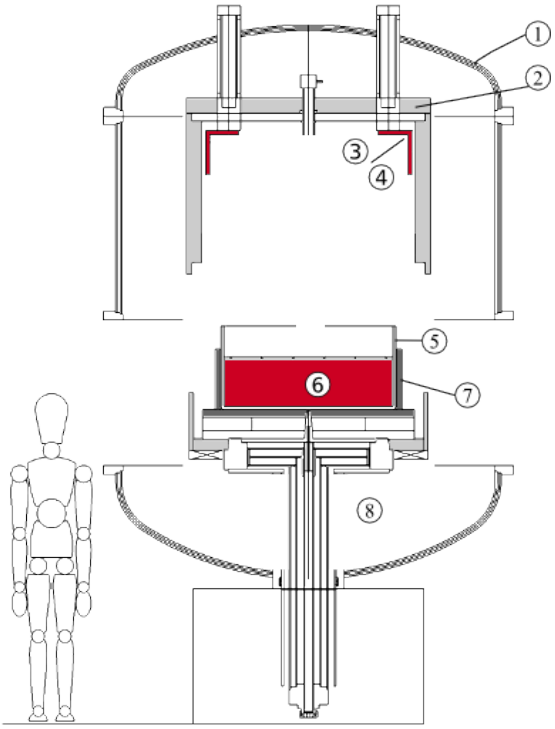

fig. 4.2: *An example section of a traditional 450kg DSS schema. (1) double wall water cooled chamber, (2) fixed thermal insulation, (3) top heater, (4) side heater, (5) quartz crucible, (6) silicon, (7) graphite base and box, (8) moving pedestral and cooling system.*

nucleation. The insulation remains open during the growth process, then is closed for annealing.

Heat is extracted through the bottom of the crucible in order to initiate solidification. Therefore, the **crystal-liquid interface** moves upwards from the bottom of the crucible. By adjusting the relative position of the crucible and insulation along with varying the heater power, the temperature gradient and growth rate are carefully controlled to favor the growth of a high quality crystal structure with vertically aligned grains. This nearly unidirectional grain growth will avoid high thermal stress and reduce the *dislocation density* in the *pSi* ingot[1]. **dislocation density**

The density of solid silicon is about 10% less than its liquid, which means that the volume of silicon will expand during growth. The directional solidification also provides the space for this expansion.

[1]Dislocations act as a recombination center and affect the electrical performance of solar cell

metal impurities

One of the other advantages of directional solidification is that the *metal impurities* will be pushed away from the crystal due to their small segregation coefficients (see pag.37). Therefore, the majority of the silicon ingot will have a quality suitable for a solar cell.

square crucibles

Moreover the *square crucibles* shape optimize the material utilization avoiding wasting scrapes as in CZ of FZ processes where the wafers can just be circular and the squaring process remove a big amount of good quality material. DSS crucibles are sized to obtain 4x4, 5x5 or more standard sized bricks (156x156 mm^2) to be sliced in wafers for PV cells realization.

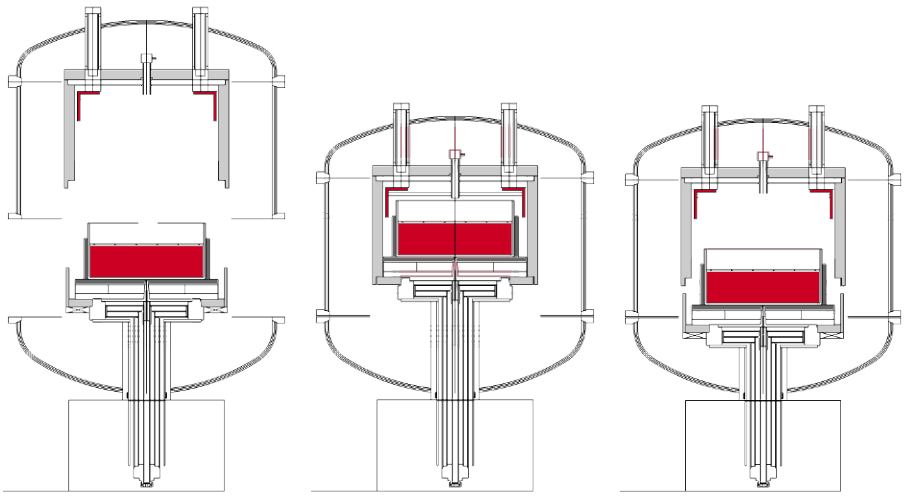

fig. 4.3: *DSS relative movements in (a) open/charging, (b) heating, and (c) cooling/solidification stages.*

4.1.1 Termal profile during the porcess

The standard thermal profile for a DSS furnace is sketched in fig.4.4. A brief description of the whole process steps can be the following:

Preparation : the quartz coated crucible has to be positioned over the DSS base and filled with the silicon chucks (60kg – 800kg). This operation has to be carefully done in order to avoid crucible damages or scratches

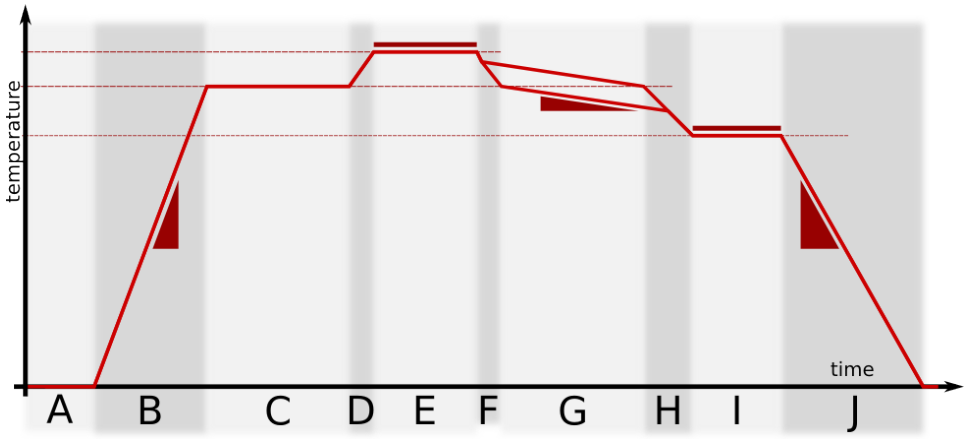

fig. 4.4: *Schematic DSS process temperature profile.*

in the coating. Once done, the graphite walls have to be built around the crucible to hold it while softened.

A - Cleaning : to remove all the possible contaminating elements and remove oxygen, the whole chamber has to be emptied using vacuum pumps to reach the highest vacuum value (0.005 – 0.5 mbar); once emptied, the chamber can be filled in inert gases (Argon or Helium) till the desired working pressure (0.02 – 1 bar)

B - Heating : all the system has to be heated up to the melting temperature with a defined maximum heating rate in order to avoid material structural cracks.

C - Melting : the time required in this step depends above all on silicon quantities, but even in sizes, and silicon kind (powder, chunks, ...).

D - Super-Heating : once the silicon is molten it is necessary to reach a higher temperature needed to create the vertical gradient (1450 – 1700°C).

E - Holding : this period is necessary to homogenize temperature, composition and to avoid the presence of small solid silicon still floating over the liquid.

F - Vertical thermal gradient : the system starts the cooling from the

bottom surface of the crucible and maintains liquid the upper parts using the top heater.

G - Solidification : once the bottom liquid surface is cooled under T_m it starts the solidification stage: the solidification rate ($10 - 20\ mm/h$) is imposed tuning the bottom cooling and the upper heating.

H - Cooling : on crystallization completion the system can be cooled

I - Relieving : is necessary to reduce internal stresses arising from differential cooling inside the ingot and to reduce dislocation creation and multiplication (see 4.1).

J - Final cooling : can be as quick as the mechanical and silicon structure can achieve but has to be controlled in order to avoid materials mechanical shocks.

4.2 DSS technical specifications

4.2.1 Thermal design

liquid-solid interface

In ingot solidification processes, the shape and the velocity of the *liquid-solid interface* is controlled by **heat fluxes** [92, 126]. This requires a specific thermal furnace design with active and passive insulation regions.

In general, the lateral heat flux through the ingot mould is responsible for the solidification **interface shape**, while the heat flux through the top and the bottom of the ingot controls the **solidification velocity**. An example of the process principle is shown in fig.4.5. An example of this influence can be seen in the schematics of the hot zones in DSS and HEM[2] shown in fig.4.6. Both of the systems extract heat through the bottom of the crucible

[2]During the growth in a DSS station, the side insulation is moved up to allow heat extraction from the bottom while the crucible remains stationary. In **Heat Exchange Method** (HEM), the crucible and the central part of the bottom insulation move downwards during growth so that the heat exchange block has a direct radiation path to the cold wall [126].

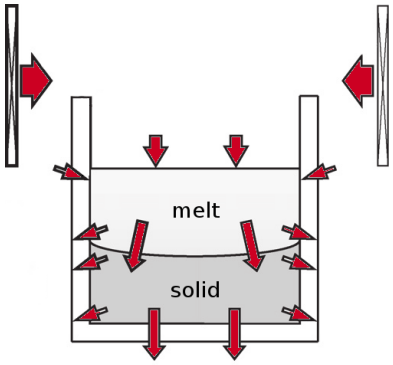

fig. 4.5: *Heat fluxes and exchanges between heaters, crucible, liquid and solid in DSS have a deep influence in solid/liquid interface shape.*

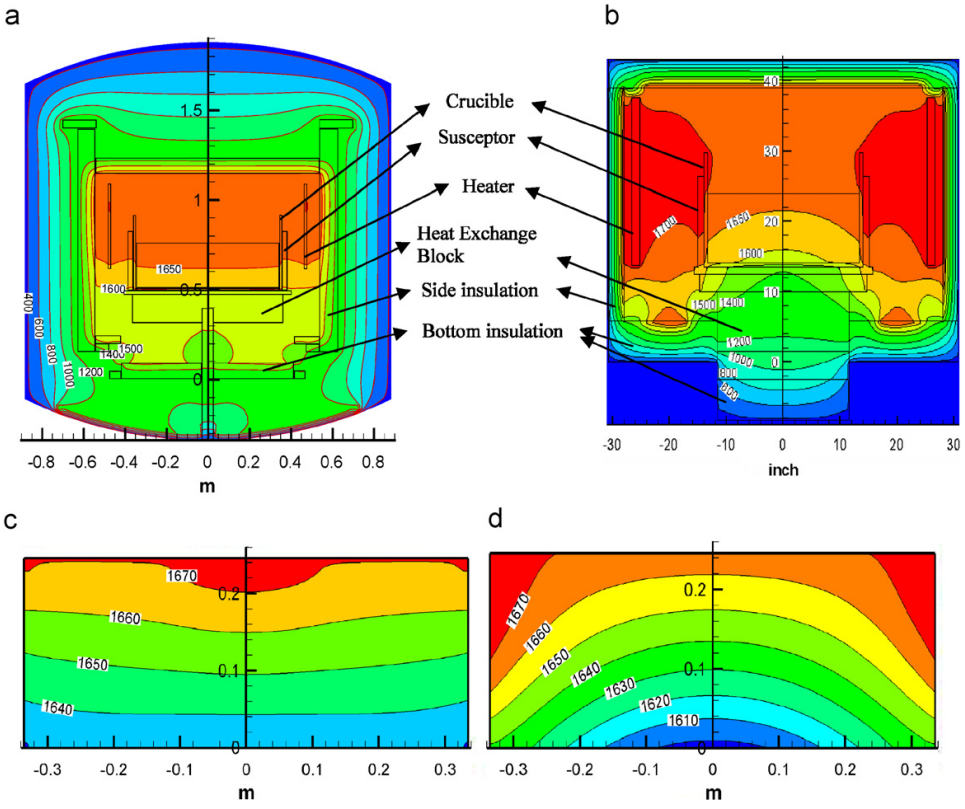

fig. 4.6: *Simulation of the global temperature profile in (a) DSS and (b) HEM and the corresponding ingot temperature profiles [126].*

in order to initiate solidification. However, the different moving parts and specific geometries of the systems lead to quite different temperature distributions. Differences in temperature profiles result in significant differences in the **shape of the solidification interfaces**: DSS isothermal solidification line is quite flat in the middle of the bath and curve upward near the

crucible. HEM presents a downward profile. There are some advantages of this outward growth direction. Firstly, it will help enlarge the grain size as growth continues. Secondly, the solidification direction is perpendicular to the solidification interface hence the segregation of impurities pushed to the corners in a slightly *convex shape* interface, leading to a reduced defect density in the crystal.

convex shape

Number, position and type of **heating sources** vary and change in the company design. Top, lateral, or bottom can be combined in order to change the thermal design.

In order to **freeze convective flows** and maintain the vertical direction in growth, a vertical temperature gradient has to be set. The higher the gradient the easier is to obtain a perfect vertical crystallization. Nevertheless high gradients means higher room temperatures with consequent complex thermal shielding, rapid material deterioration, higher maintenance costs an so on. Standard values[3] for 450kg DSS are in the range of $2 - 5\ K/cm$.

Because of the 10% higher density of molten silicon in comparison with the solid phase, a solidification of the top region of the ingot has to be prevented under any circumstance during the ongoing crystallization. Otherwise, enclosed solidifying melt can cause a crack on the mould and an outburst of liquid silicon into the furnace.

After total solidification of the ingot, the cooling down to room temperature requires low thermal gradients inside the ingot to prevent the generation of *thermal stress*. This stress can raise the value of crystal defects, like dislocations, which are known to limit the solar cell efficiency [57].

thermal stress

Summarizing the general aspects of DS thermal design, the most important parameters that have to be controlled during the process, and therefore, to be investigated by numerical simulations are:

- the **melting rate**
- the crystallization **velocity**

[3]Smaller laboratory systems can impose a higher gradient (up to $15 - 20\ K/cm$) on smaller silicon quantities due to the small ingots height.

- the **shape** of the solidification front

4.2.2 Vacuum and Atmosphere

Due to the high chemical reactivity of the molten silicon at high temperature the whole melting and solidification process have to be performed in *inert atmosphere*. Moreover all the graphite components (insulation, susceptors, box, heaters, etc.) react with oxygen at temperature higher than 400°C reducing the consumables lifetime [63]. The materials design and choice (see 4.2.3) has to take into account the vacuum and process compatibility.

inert atmosphere

Thus is necessary to clean the chamber in the initial process step in order to remove as much **oxygen** as possible. Once the required conditions are obtained, the chamber is filled in inert gasses up to the working pressure value depending on the recipes used. A **continuous gas flow** is necessary not only to keep clean from oxygen flowing though vacuum chamber possible leakeges but even to remove SiO originated from the crucible and evaporating from the free liquid surface. Otherwise the formation of a skull may reduce the heat flux from the top, cooling the upper part of the melt and leading to a undesired and dangerous crystallization from the top.

The commercial DSSs have a double vacuum pumping station in order to clean the chamber with various combinations and capacities [23, 22]. The inert gasses type (Ar or He), pressure (1 – 6 bar), consumption and flow (0.05 – 200 m^3/min) vary from company to company.

4.2.3 Materials

Materials design in DSSs is quite complex due to some technical aspects of the process and some limitations:

- very high temperature reached during the melting phase (up to 1800°C)
- aggressive atmosphere with SiO, SiO_2, Si, etc.
- chemical compatibility with the process (no metals or foreign element have to be released during the process) to maintain the silicon quality

- vacuum (no closed porosity, degassing or evaporation)
- cost
- durability
- easy maintenance

Graphite is normally used both as insulation and heating system. It as good resistance up to 3000°C and can be tailored in order to obtain lot of different characteristic :

- **isostatic graphite** has good mechanical properties and can be used in structural components for the box and the bottom plate
- **CFC** carbon fiber composite can be shaped in a variety of design to define mechanically excellent detail as bolt, shielding, L-shaped profile, tubes, etc.
- **rigid graphite felts** (rigid carbon fiber complex structures with a low density and thermal conductivity) can be used as thermal insulation
- **flexible graphite felts** cover are used to create a reactive shielding in the bottom chamber shell: in case of crucible breakage and silicon run-out, the bottom vessel can contain all the melt and the silicon wets and reacts with the felt producing a very strong and protective SiC skull

4.2.4 Safety

The management of 450kg reactive liquid silicon at 1500°C is a quite complex problem for safety and can be potentially dangerous. The *risk tree* have to be taken into account in the engineering design and safety procedures. Active and passive protections have to be designed in order to avoid at first people hurts and secondly to prevent system damages.

risk tree

If the unlikely (but possible and not unusual) event of a crucible breakage occurs, a large quantity of high temperature material may flow outside the crucible, leading in the worst case to a possible **explosion**. In particular,

the main risk in this kind of devices is silicon/water esothermal reaction:

$$Si + 2H_2O \rightarrow SiO_2 + 2H_2 \tag{4.1}$$

leading to temperature increase and hydrogen creation usually connected to an sudden and rapid increase in pressure. Water is normally used to cool the double-walled chamber and as a cooling medium for the bottom heat/exchanger. Any water leakages have to be prevented (checking welding, corrosion, heat cycle embrittlement, structural damages as graphite oxidation, etc.) and the device design has to avoid the silicon water contact in case of crucible breakage by the creation of specific path and shielding for molten silicon.

The system control (4.2.5) has to monitorize the process temperature, pressure variation, oxygen content, leakage detection devices, and all the parameters to check the normal process and to implement the emergency procedures.

High temperature insulation, liquid silicon confinement paths, water-cooled zones design and position, thermal shields, and others passive protections have to be designed.

4.2.5 Process Control

The possibility to monitorize and control the whole melting and solidification process is crucial for the DSSs end users. Each *pSi* producer has his own "**recipe**" to implement related to the feedstock quality, form, quantity, etc.

An industrial computer has to manage the whole system:

- power sources switching and regulation
- temperature profile definition and measurement using pyrometers and thermocouples
- vacuum management (pumps) and measurements
- gasses flow and switching control

- mechanical positioning (chamber open/close, heat exchanger or crucible)
- water cooling system (pumps, pressure, chiller, towers, etc.)

are just few of the parameters to be set and continuously controlled.

All the active safety procedures (see 4.2.4) and emergencies management has to be defined and implemented in the control system as:

- electrical black-out (UPS, alternative electrical power supply)
- absence of cooling water (emergency chillers and pumps)
- crucible breakage
- temperature and pressure increase
- ...

4.2.6 DSS outlook

To avoid the costy consumable quartz crucibles it is possible to cast directly the silicon ingot into a **graphite crucible** inductively heated. The earlier casting experiments were performed in this kind of containers [29]. The material properties have to be compatible with Silicon thermal expansion in order to avoid crack during solidification, impurities contamination distribution coming from carbon crucible also has to be evaluated.

To improve the thermal design a new special crucible has been developed and patented by *Apollon Solar* and *Cyberstar* [79, 84, 50]: the crucible is assembled with four lateral IR opaque quartz sides and a bottom in transparent quartz. Consequently the vertical thermal gradient can be easily maintained because the lateral heat dissipation is limited to conduction [81].

To improve the crystal orientations it is possible to use a *mSi* "seed" base plate in the bottom of the crucible in order to impose the crystallization

growth starting from a defined crystallographic plane [58]. In this way it should be possible to have equiaxial growth in all the ingot section.

5

*i*nduction Direction Solidification Systems

Any sufficiently advanced technology
is indistinguishable from magic.

A. C. Clarke

Due to the feedstock amount over the solar cells final cost, the production of low-cost and high quality silicon in photovoltaic application is a main topic in PV industrial research (fig.5.1). The large grained columnar poly-crystalline silicon (*pSi*) obtained via *Directional Solidification Systems* (DSS) was found to be a convenient alternative to the expensive mono crystal (*mSi*) obtained via Czochralski: production costs are much lower and the solar cells efficiency has been significantly increased in the last years (fig.3.15).

Among the main manufacturers of DSS systems the traditional resistance

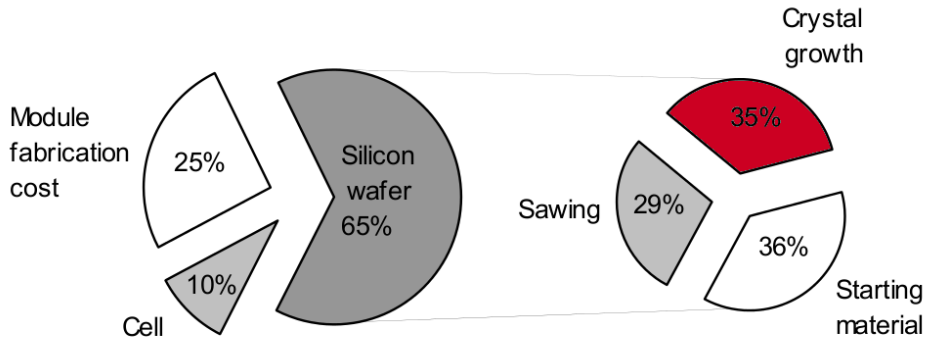

fig. 5.1: *Costs distribution for a pSi PV module and the subdivision for the wafer production [74, 114].*

heating is used both in the phase of melting the raw silicon and in the phase of re-crystallization in order to maintain the proper temperature gradient between the top and the bottom of the crucible. The *induction heating* technology could be a valid option, but only few manufacturers use it [25].

induction heating

Though induction is a well known industrial technology used in lot of different applications (see chapter 1) with higher performances and capabilities compared to resistive heating, just few companies developed an induction directional solidification for silicon casting and the market is still fully oriented in the traditional systems.

Some disadvantages in the ***induction*** **Directional Solidification System** (*iDSS*) can be in the initial financial investment and in a kind of inertia to switch from a traditional and improved technology to a "new" one. On the other hand, lot of laboratories and research centers all around the world are already using small size systems based on induction because of their flexibility and capabilities.

iDSS

In 2008, after a preliminary economical and technical planning made in collaboration with the UCLA (University of California, Los Angeles), a collaboration has been established between the ElectroHeat Laboratory of the University of Padova, Inova Lab (a spin-off company of the same department), and SAET industrial group to study, design, and developed a

DSS prototype based on induction heating: "*iDSS project*". **iDSS project**

This chapter is a general description of this project development, simulations, economical and technical aspects. Not all the details and specifications will be described in order to meet some industrial confidential agreements signed with companies involved into the project.

5.1 DSS: induction and resistive heating

The aim of this section is a comparison between the two different technologies used in DSS for the production of *pSi* ingots: **electric resistors** and **induction furnaces**. The former is a well known and widely used technology. The latter is increasing in interest and possibilities in the last years.

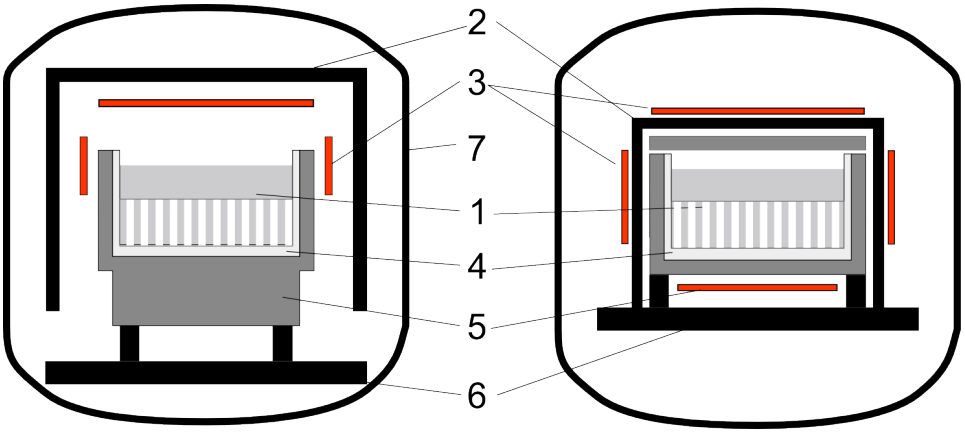

fig. 5.2: *Comparison schema between traditional and inductive DSSs. (1) silicon, (2) thermal insulation, (3) heating elements resistors/inductors, (4) crucible, (5) cooling base, and (6) insulation base [25].*

5.1.1 Resistive DSS features

Traditional DSSs are designed to fit the radiative thermal exchange (IR) system limitations and requirements. One of the main drawback is that the radiating heating elements are not "directional" or selective thus heat is

dissipated all around in the furnace surfaces. Moreover the thermal fluxes are strongly dependent on the "view factor"[1] and the heaters must have a complex design to have a uniform temperature profile.

The **process control parameters** during heating and cooling are just the upper heater power and the relative position between heaters and box. Due to the heaters and masses thermal inertia the system controllability and tuning is slow and not reactive (once switched off, the temperature slowly decrease but still radiating). The possibility to tune or change thermal profile is far to be simple.

Almost 30% over the total time necessary for the complete manufacturing of the ingot (which typically is in the range of 55 to 65 hours for a 450kg DSS) an important part is covered by the melting and homogenization phases. This time is required to heat up the system, melt and hold the temperature before solidification. In order to achieve the melting temperature, the resistors should be heated at least up to 1500-1600°C with a lot of **thermal losses** which must be dissipated by the vacuum chamber walls.

The most important phase, the directional solidification, is obtained imposing a vertical temperature gradient (5-10°C/cm) using the heat flux from the upper heater. IR thermal flux require a temperature differency[2] between the source and the target. Thus to maintain the necessary radiative heat exchange the the upper resistors have to reach higher temperature, near to 1700-1800°C, with an increase in thermal losses.

Maintenance costs

Maintenance costs and repairs in graphite or carbon nitride resistors is quite high. All those components have a short life-time because of the chemical **aggressive atmosphere** (Si, SiO, SiO_2, etc.) and the thermal cycling consumption (usually all the graphite components and heaters have to be changed every 1 – 2 years).

[1] The IR thermal flux exchanged between two element surfaces depends on their relative position and obstacles between them. The *view factor* is the adimensional parameter describing the heat percentage exchanged per unit of area.

[2] The IR thermal flux between two infinite facing surfaces is $q_{1-2} = \sigma\epsilon(T_2^4 - T_1^4)$ depending strongly to the temperatures difference.

In order to increase the efficiency of the process some manufacturers are developing new furnaces capable to produce **bigger ingots**. Some Chinese firms like JYT are developing e new furnace (JZ-660) capable of casting ingots up to 800 kg; the European ECM has declared to be ready for the next year with a furnace capable of casting 600 kg ingots. The innovation proposed by all these companies are in the direction to produce a scale economy of the process, but a real innovation regarding the technology used or the variation of process main parameters is difficult to be accepted by the manufacturers and customers. If we compare the furnaces of the main DSS manufacturers in the world they differ only for some details [27]. IR is a very efficient surface-to-surface heat transfer but this feature limits the internal ingot heating capability requiring longer time for the conductive transfer. In the direction of *increasing ingots size*, a more efficient internal source should be preferred.

increasing ingots size

The main drawbacks of DSS resistors furnaces can hence be summarized as follows:

- A big vacuum chamber because of the need to reduce the high thermal losses due to radiation of resistors at high temperature (1600-1700°C);
- A long heating and melting time due to the low specific power available in the range of 5-10 W/cm^2;
- A big consumption of energy for the radiation losses during heating, melting and solidification
- The high operation temperature of resistors reduces their lifetime and hence there is the need to frequent substitutions.

5.1.2 Induction features

The idea of using induction technology is not new in DSS furnaces: a lot of patents regarding the use of classical induction heating or melting and cold crucible for continuous casting of silicon are known. Despite the feasibility of the process only few (one or two) manufacturers are proposing to the market DSS furnaces with induction technology. The reason of this limited diffusion

of induction DSS furnaces could be related to the knowledge needed to design the heating system constituted by a frequency converter, capacitors, transformers and inductors which is more complex than the resistors heating system.

The iDSS design and features are the same of a traditional system but based on the induction possibilities and limitations. Some of these are here summarized.

standard design

To be inductively heated the susceptors have to be realized in an electrically conductive material; the isostatic graphite structures used in the traditional systems can be used leaving the "*standard design*" of some consumables as the graphite box. This is an important feature in order to avoid a complete re-design and be more attractive to the market. The possibilities to have a system as similar to the standard as possible has to be taken into account in the project. Production industrial plants are optimized and equipped for specific procedures connected to the silicon charging, process management, and so on over traditional systems.

hot-zone

The design of the *hot-zone* is completely different (see fig.5.2) because induction is an **indirect heating** method. A proper thermal shielding between inductors and susceptors have to be realized in order to protect inductors from high temperature and at the same time to direct the heat generated by the eddy currents toward the silicon.

Nevertheless it is not possible to use a too thick insulation because of the electrical efficiency of the system: in induction heating devices the **gap** between **inductors and susceptors** has to be as small as possible in order to have a better coupling and a higher energy transfer.

Those conditions impose a very **small hot-zone** compared to the standard one where the heaters have to be in the between of insulation and susceptors. This reduces the insulation dimensions, the high temperature zones and the surface, reducing in such a way the thermal losses. Shortening the time and lowering the temperatures the consumed energy can be drastically reduced.

To increase the **heating rate** and the global system controllability an induction DSS furnace can be constituted by three different inductors which can be placed on the bottom, on the top and on the sides of the graphite susceptors constituting the box containing the crucible as shown in fig.5.4(b).

The induction specific feature to put heat sources directly into defined zones by a proper inductors design can be used to optimize the **thermal maps** and to obtain the desired thermal profile. For instance, the side inductor can be used to control the cooling in such a way to compensate the lateral thermal losses to create an *active adiabatic insulation* able to guarantee a perfect vertical heat flow or to shape the solid/liquid interface as discussed in 4.1.

active adiabatic insulation

Contrary to the slow resistor system, induced power into the susceptors can be tuned and switched on and off instantaneously just controlling the power supply. In the same way tuning frequencies and voltage inductors can be used for **electromagnetic stirring** as in fig.5.3 in melting and holding steps. With the same flexible power system is even possible to generate heat directly inside the silicon at temperature higher than 800°C when the electrical conductivity became comparable to a metal. This leads to an increase in melting speed by reducing the conduction transfer and increasing the efficiency.

One of the main drawback is that inductors copper tubes have to be cooled to dissipate the internally generated heating introducing a new potentially **dangerous water source** in the system. On the other hand these cold heat-sources can be used to cool the structure itself keeping all the external zone to lower temperature and avoiding the expensive chamber double wall. For the same reason the bottom inductor can be designed in such a way to be a perfect cooling surface for thermal exchange acting both as a heat source and cooler. Finally an inductor is a very simple “mechanical” component operating at very low temperature and for this reason its lifetime can be considered unlimited.

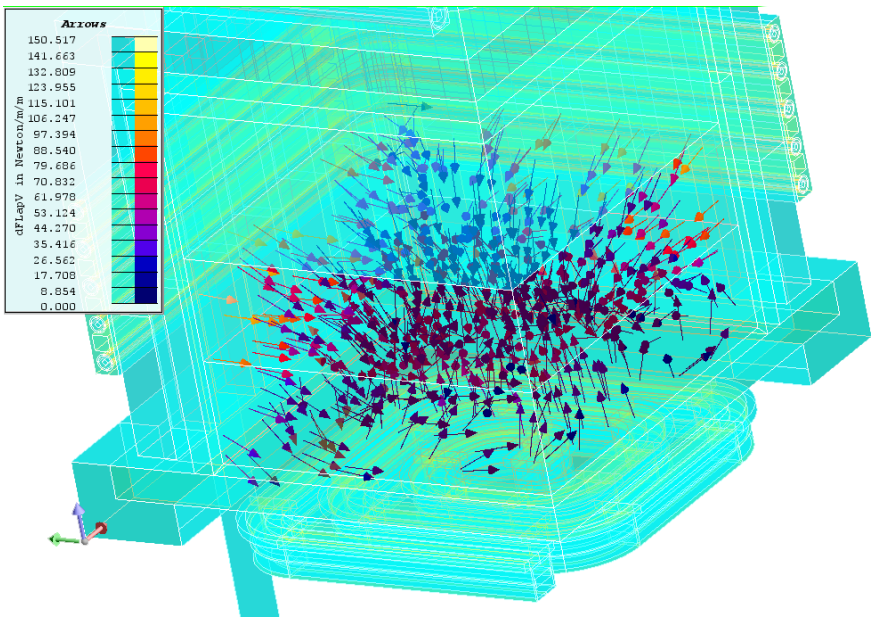

fig. 5.3: *Simulation of the electromagnetic stirring effect in the first system configuration. Lorentz's forces induced into the molten silicon.*

5.2 Simulations

The direct experimental studies are extremely laborious and expensive because of high temperatures typical of this process (up to 1700°C). Detailed measurements of the temperature field are almost impossible due to technical and physical limitations. System optimization would be too expensive. Mathematical modeling may significantly shorten the time of technological prototyping, narrow the search range for the optimal parameters, decrease expenses, and provide a qualitative estimate for any design. Therefore, numerical simulation is very important and urgent even for the ideal process of growing.

Nowadays *Computer Aided Design* (CAE) packages can manage almost all the physical phenomena. Commercial multi-physic softwares have been heavily used in the project in mechanical, thermal, electromagnetic, and fluid dynamic design.

5.2.1 Geometry

Using the "standard" DSS structure as base to the mechanical and thermal design the new starting geometry has been defined as in fig.5.4(a).

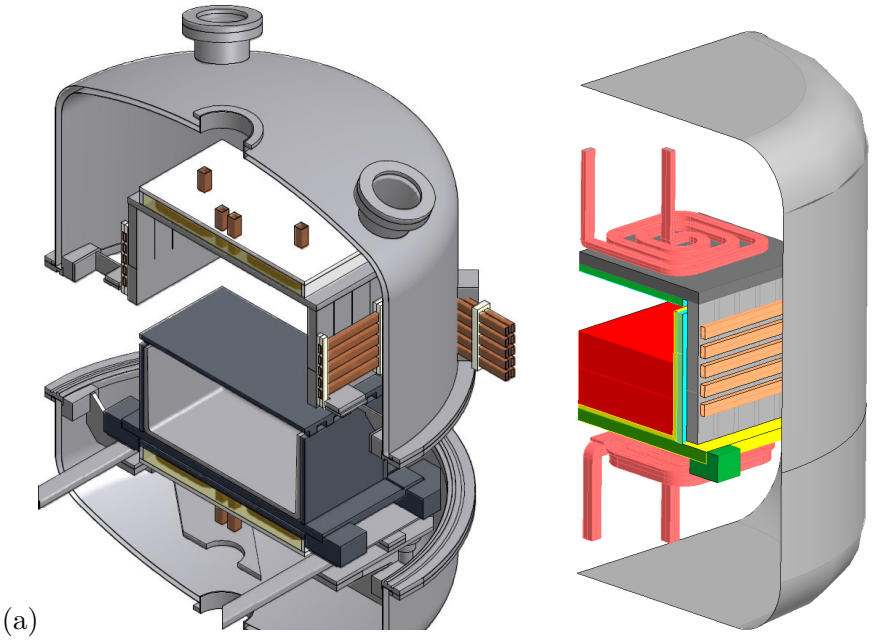

(a) (b)

fig. 5.4: *CAD project view and* 1/4 *FEM model section.*

5.2.2 Materials properties

Silicon is a semiconductor with a melting point around 1420°C and it requires 1411 kJ/kg to be molten. At room temperature silicon is an electrical insulator, **electrical resistivity** decreases with temperature and up to 800°C material can be heated directly by induction (fig.5.5). A visible gap in ρ between solid and liquid phases is an interesting feature to be taken into account. Thermal and electrical properties (fig.5.5, fig.5.6, and fig.5.7) vary in literature and can vary depending on the feedstock type and quality.

Materials properties used in simulations are a compromise between real values with temperature and complex dependencies and the computational

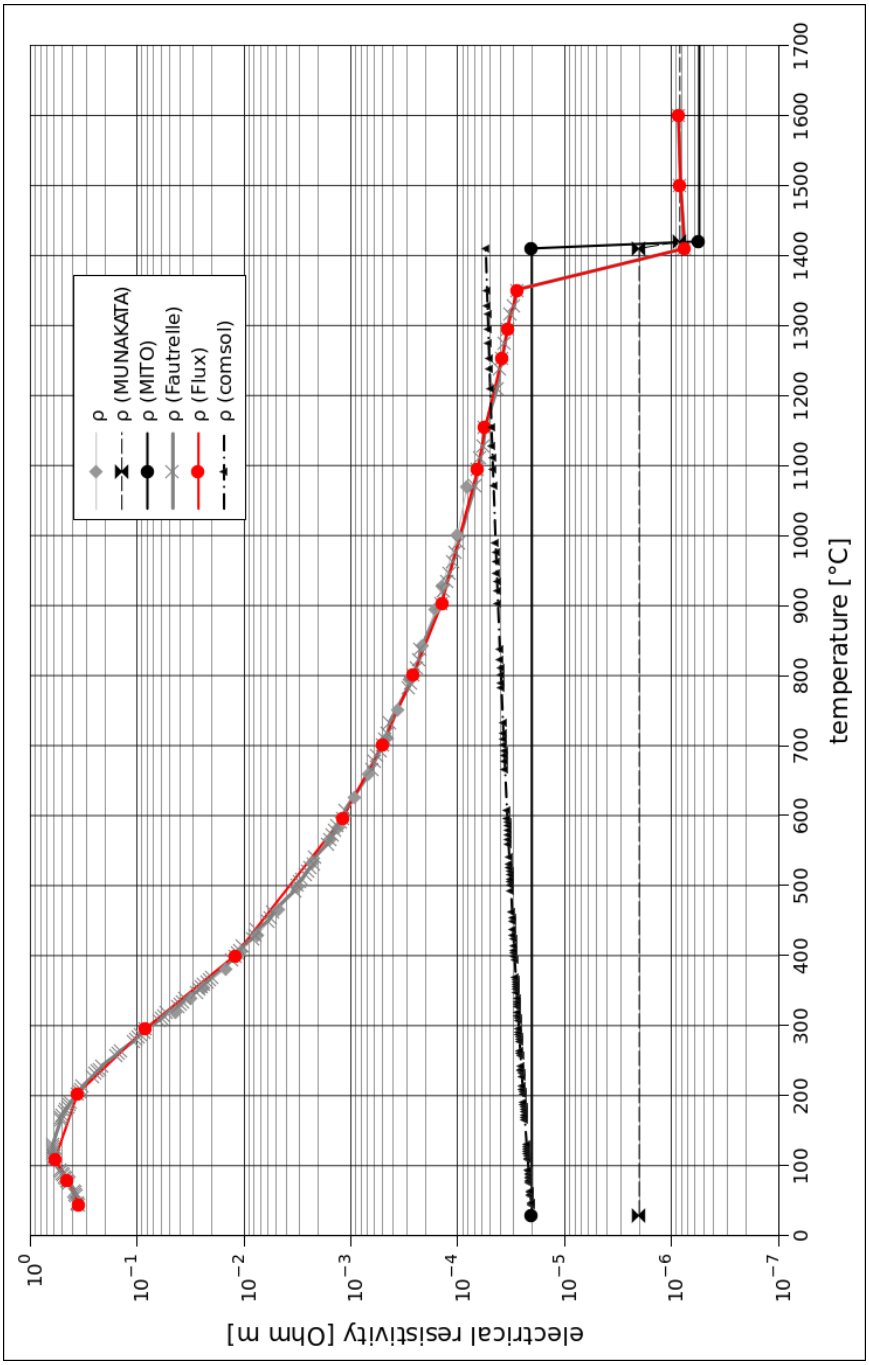

fig. 5.5: *Silicon electrical resistivity ρ dependency with temperature in solid and liquid phase according to different authors.*

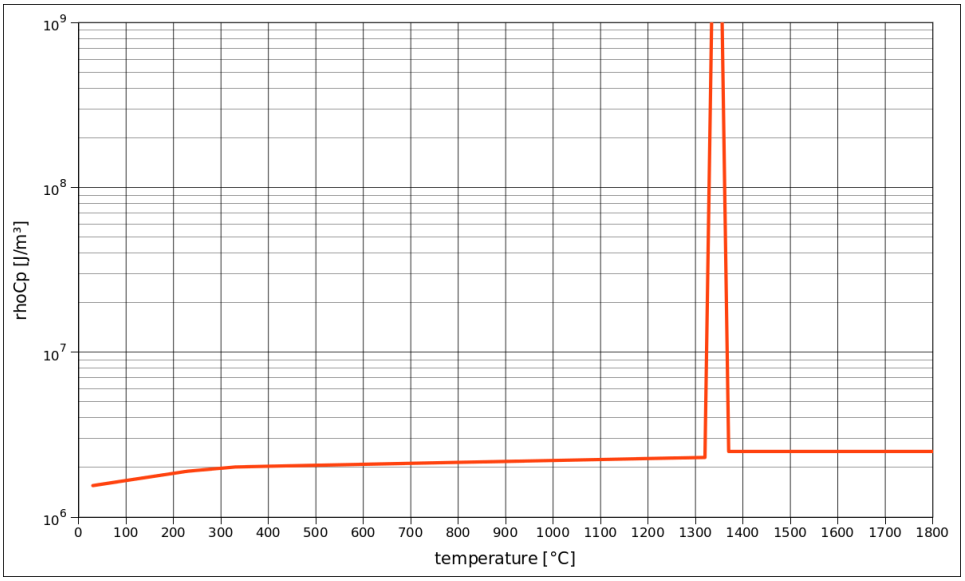

fig. 5.6: *Silicon volumic specific heat ρC_p dependency with temperature in solid and liquid phase. Curve used in thermal non-linear simulations. The latent melting heat is simulated as a peak in the specific heat around the melting point.*

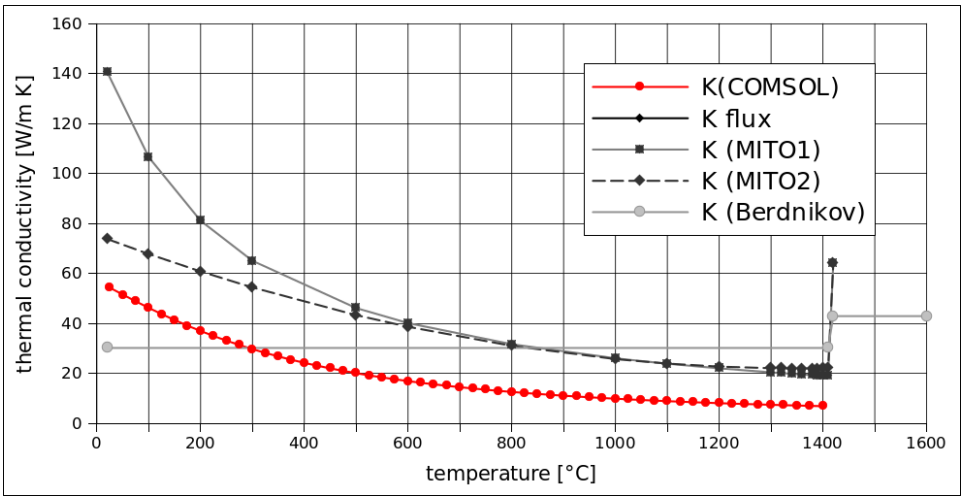

fig. 5.7: *Silicon thermal conductivity k dependency with temperature in solid and liquid phase according to different authors.*

time required to solve a FEM model. Each non-linear property used can give a better result but real multi-physical models are very complex to be "usable" in engineering design. Simplified models can give the hint to understand the problem and solve it in shorter time.

property	UM	**solid**	**melt**	**quartz**	**susceptors**	**insulators**
density	kg/m^3	2300	2500	2190	2260	1800
thermal conductivity	W/mK	26	54	5	40	0.7
heat capacity	J/kgK	950	1000	1525	2050	1800
emissivity	-	0.6	0.3	0.5	0.8	0.8
electrical resistivity	Ωm	fig.**??**	8010^{-8}	-	95010^{-8}	-

Table 5.1: *Some of the material properties used in simulations [94, 85, 11, 97, 91, 112, 20, 59, 120, 63]*

5.2.3 Thermal simulations

The ideal thermal profile and the position of the solid/liquid interface can be calculated using a simple one-dimensional heat transfer model, where it is assumed that all the heat is transferred through the crucible bottom [81, 101]. As shown in fig.5.8 solidification rate, imposed thermal gradient, and geometrical parameters are used to evaluate temperatures and fluxes.

The heat flux $q_{PC}[W/m^2]$ released during solidification phase-change can be calculated as:

$$q_{PC} = v \cdot \delta \cdot \Delta H \tag{5.1}$$

where $v[m/s]$ is the solidification rate, $\delta[kg/m^3]$ is the density, and $\Delta H[J/kg]$ is the latent heat. Solid and liquid fluxes:

$$q_L = k_L \cdot \nabla T_L = k_L \cdot \frac{(T_{surf} - T_{melt})}{h_L} \tag{5.2}$$

and

$$q_S = q_L + q_{PC} = k_S \cdot \frac{(T_{melt} - T_{bott})}{h_S} \tag{5.3}$$

where $k[W/m^2K]$ are the thermal conductivities, $h_S[m] = v \cdot t$ is the ingot height, $h_L = h - v \cdot t$ is the liquid height, and $T[K]$ are the temperatures as described in fig.5.8.

Using these relations is possible either to calculate fluxes and temperatures defining solidification speed or conversely to estimate the solid/liquid front position from temperature measurements [101, 19].

After the electromagnetic design and the power sources estimation some 3D thermal simulations have been implemented to understand temperature

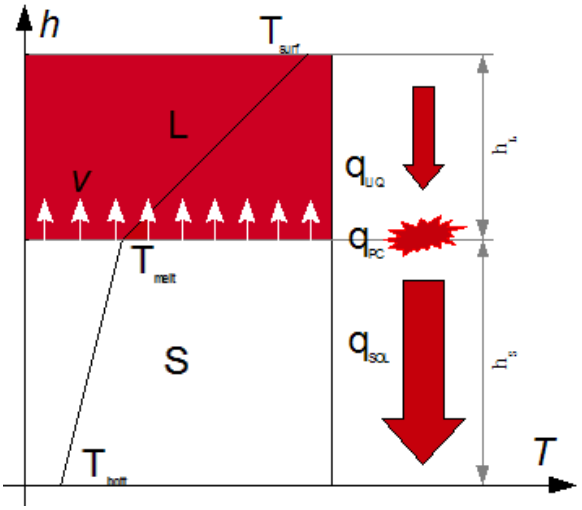

fig. 5.8: *Ideal thermal setting between top free liquid surface and bottom solid silicon.*

profile and give some hints about materials and insulation to be used. This simple model doesn't take into account the IR thermal exchange but some tricks have been used to simulate this flux [102]. The thermal conditions set are:

- isothermal surface for the water-cooled external chamber wall
- molten silicon at 1450°C
- power density maps from electromagnetic simulations
- steady state and transient analysis

Some results used in the project design are in figs.5.9.

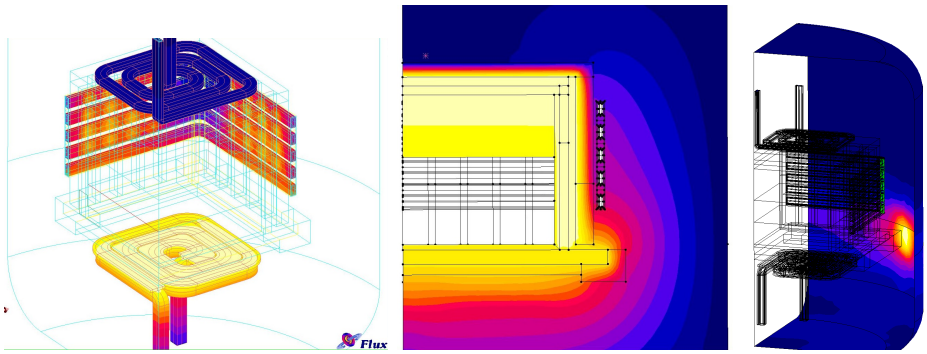

fig. 5.9: *Thermal simulations results (a) inductors maximum temperatures, (b) thermal map for insulation design, (c) steel chamber shell thermal fluxes.*

5.2.4 Electromagnetic simulations

The electromagnetic simulations were developed using the Cedrat *Flux* CAE package. 2D and 3D electromagnetic and thermal couplings have been done in order to have maximum efficiency and heat distribution.

inductors design

In the *inductors design* process (some evolutions of the upper inductor are shown in fig.5.10) required a strict collaboration between different teams and skills: process requirements, simulations, power electronics, fluidic, and inductors realization team. Electrical and fluidical connections, shape and

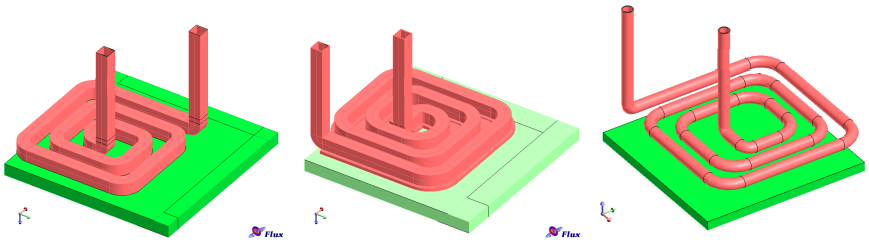

fig. 5.10: *Some steps of the inductors design process.*

size of copper tubes, the relative position to the susceptors, process safety and mechanical feasibility have been discussed and modelized. The final inductors result is shown in fig.5.11.

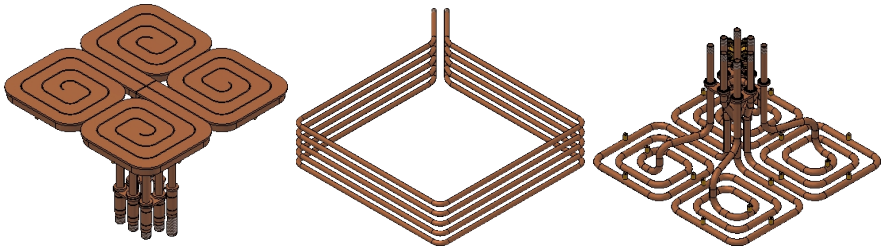

fig. 5.11: *Inductors final design (bottom, lateral, and top).*

power supply

To design and realize the *power supply* some technical data are required by the power electronics and electric teams. The system impedance calculations are necessary to design the power generators, capacitors, autotransformer, and power balance systems. Parametric simulation analysis is

useful to optimize the **frequencies** (see fig.5.12) in order to maximize the transferred power and the efficiency.

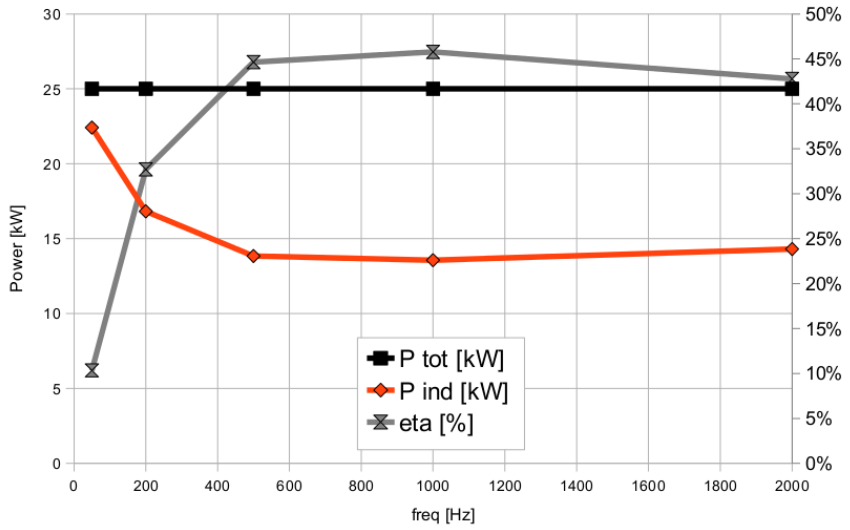

fig. 5.12: *Power induced into graphite and lost into inductors and efficiency parametrized over frequency to optimize the bottom inductor.*

To increase the DSS control flexibility, each of the turn constituting the side inductor can be switched on and off. In such a way it is possible to implement the "**active insulation**". Coils switched off are set in a short-circuit condition in order to create a EM shield and confine the induced power into the designed zones (see fig.**??**). Doing that the total impedance changes and it is necessary to change electrical configuration to set the system.

The aim to have a uniform temperature distribution over the susceptor and to avoid thermal gradients and fluid flow imposes the design of the upper and lower inductors (fig.5.11(c) and 5.11(a)). Due to some geometrical and process constrains these are designed in a "pancake" shape, *ie* a spiral facing the susceptor. The four pancake-tubes can be electrically connected in different configurations where current flows in relative different directions (see fig.5.14). In the three possible cases the electromagnetic configuration changes and the induced power too (see fig.5.15).

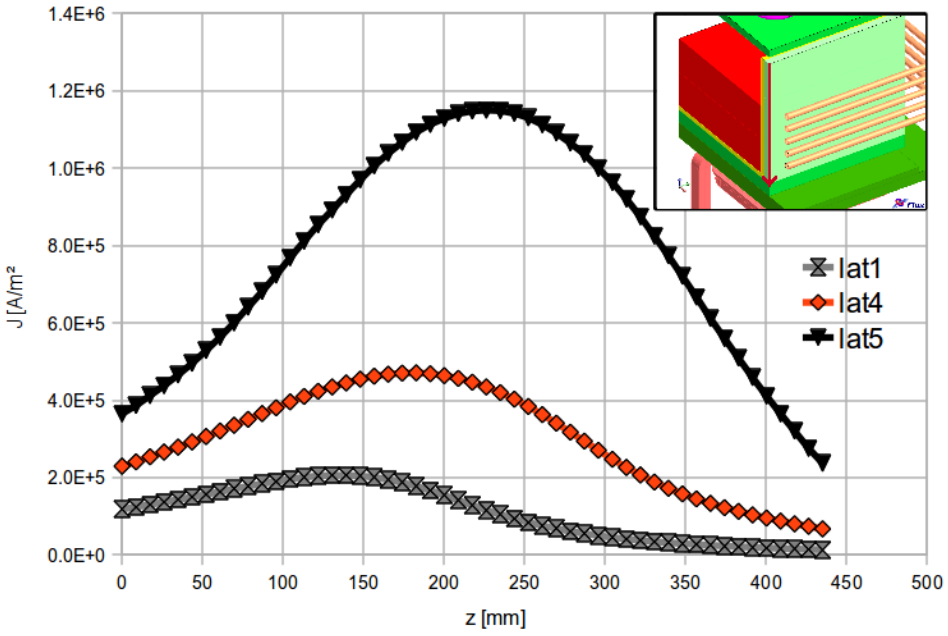

fig. 5.13: *Eddy currents density along a vertical path induced into the side susceptor by switching off some turns.*

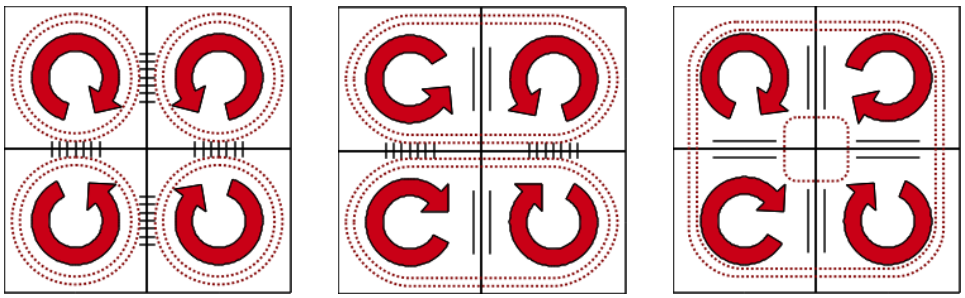

fig. 5.14: *Inductors connection schema (NN, TN, TT). Arrows describe the pancake current direction, dotted lines are induced current paths, and the continuous lines show the magnetic field condition imposed as boundary (N and T stand for "normal" and "tangential" magnetic fields).*

5.2.5 Fluid-dynamics simulations

The thermal design has been further developed to take into account all the mass and energy transport phenomena [13, 12]. The multi-physics model in fig.5.16 is an axy-symmetric geometrical equivalent to the squared

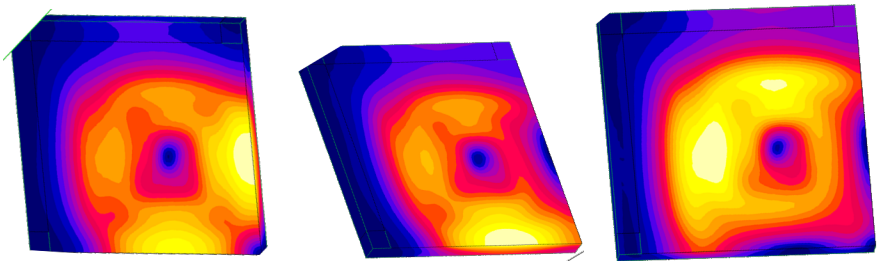

fig. 5.15: *Current density induced into the graphite susceptor using different inductors connection (NN, TN, TT).*

ones designed. Liquid silicon fluid flow, thermal conduction, radiative heat

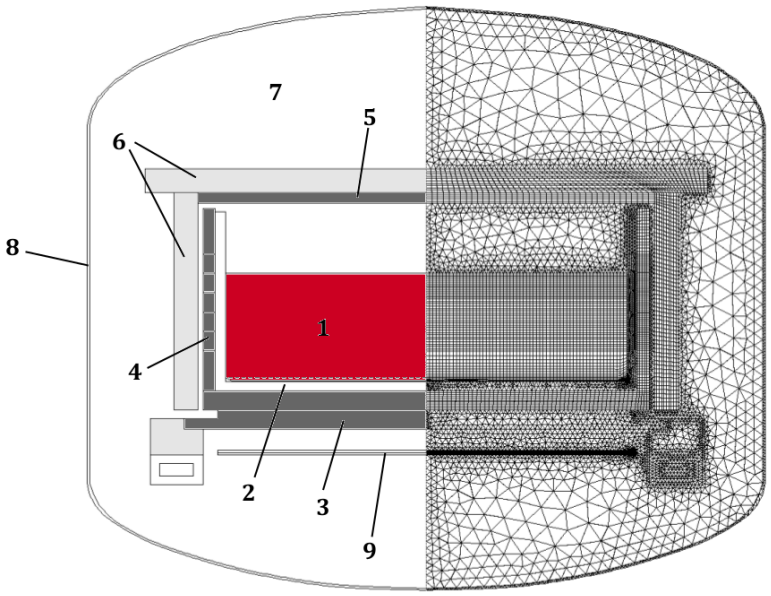

fig. 5.16: *iDSS 2D model and mesh for the CFD simulations. (1) silicon, (2) quartz crucible, (3) bottom susceptor, (4) lateral susceptor, (5) top susceptor, (6) insulation, (7) vacuum zone, (8) water cooled chamber, and (9) heat exchange bottom inductor [61].*

exchange between all gray and diffusive surfaces in the furnace, gasses convective exchanges, phase changes, and external heat sources are considered in this simulation (fig.5.17 and 5.18) [61].

The governing equations are the **mass balance**, **momentum conser-**

vation, and the **energy conservation**:

$$\dot{\rho_i} + \nabla(\rho_i \vec{u_i}) = 0 \tag{5.4}$$

$$\frac{\partial \rho_i \vec{u_i}}{\partial t} + (\vec{u_i} \cdot \nabla)\rho_i \vec{u_i} = -\nabla \rho_i + \nabla \tau_{\mathbf{i}} + (\rho_i - \rho_{i,0})\vec{g} \tag{5.5}$$

$$\frac{\partial \rho_i C_{p,i} T_i}{\partial t} + \rho_i C_{p,i} \vec{u_i} \cdot \nabla T_i = \nabla \cdot (k_i \nabla T_i) - \nabla q_{rad} + S_T \tag{5.6}$$

where $\rho[kg/m^3]$ is the density, $\vec{u}[m/s]$ is the velocity, $\tau[Pa]$ is the stress tensor matrix, $\vec{g}[N/kg]$ is the specific gravity, $C_p[J/kgK]$ is the specific heat, $T[K]$ the temperature, $k[W/mK]$ is the thermal conductivity, $q_{rad}[W/m^2]$ is the radiative flux, and $S_T[W/m^3]$ are the thermal sources.

To evaluate the **radiative heat exchange** a specific module is implemented in the CAE package to trace the surface-to-surface effects. Each surface element flux $q^{IN}[W/m^2]$ is calculated using:

$$q_i^{IN} = \sum_j F_{ij} \left(\epsilon_j \sigma T^4 + (1 - \epsilon_j) q_j^{IN} \right) \tag{5.7}$$

where $\epsilon[-]$ is the material emissivity, $T[K]$ the temperature, $\sigma = 5.6710^{-8} W/m^2 K^4$ is the Stefan-Boltzman constant, and F_{ij} is the view-factor between the two surface elements.

Some relations and equations are in chapter 2.

To solve the fluid-dynamic problem a RANS solver has been used in order to take into account the unstable flow behavior [14, 133, 134, 53].

By means of this information it is possible to:

- optimize the power load variation in time
- control the solidification rate (fig.5.19)
- define the thermal setting to shape the solid/liquid interface to convex
- evaluate the heat fluxes and design the cooling system
- evaluate the thermal losses and the global thermal efficiency of the system
- study the argon flow and re-design the inlet in order to keep clean the silicon surface
- have a map of the impurities concentrations in the ingot by using diffusion simulations coupled with thermal and fluid dynamic ones

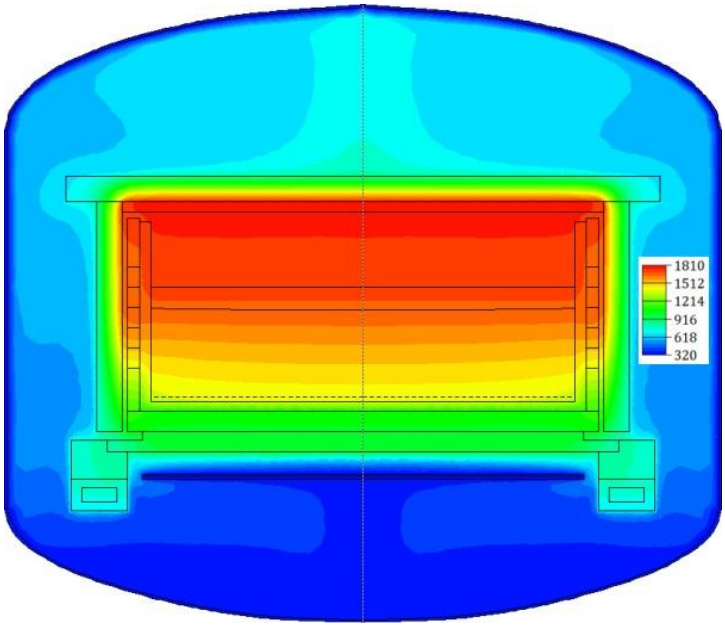

fig. 5.17: *Global temperature [K] distibution evaluated in fluid dynamic CAE software.*

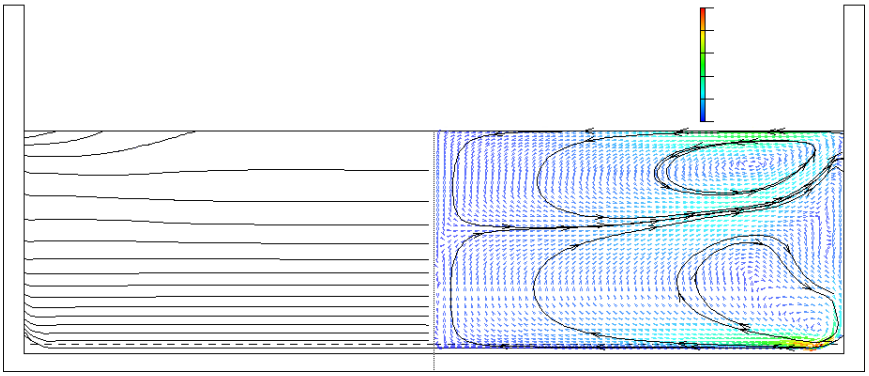

fig. 5.18: *Temperature and fluid flow at the beginning of the solidification process.*

5.3 Prototype construction

At the beginning of 2010 the project landed to the **realization** stage.

The iDSS prototype has been realized in the SAET Group facility plant in Leiní (Torino) where all the engineers and technicians involved into the project are.

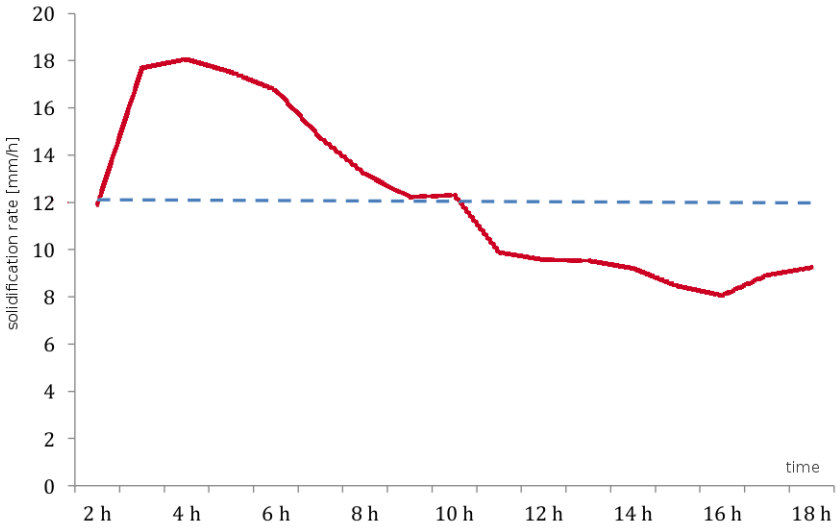

fig. 5.19: *Solidification rate changing during the process.*

SAET Group

SAET Group (founded in 1966) is a worldwide company specialized in design and manufacturing of induction heating production solutions. All the skills required form the initial design to the practical realization of a such a complex device are available inside the group (R&D, mechanical, fluidic, inductor design, power electronics, electric, software, purchase, and productions departments).

5.3.1 Machine set-up

Once completed the first global design, the construction phase showed some features to be re-designed and difficulties and problems mainly connected to vacuum and high temperatures.

prototype

The *prototype* is approximately 4m wide, 5m in height, and 8m in "charging" configuration with the bottom part of the chamber extracted.

Other unique feature in iDSS is the design and realization of the inductors **electrical feed-through**. Standard system power supply is a 50-60Hz using standard connection to cross the chamber double wall. Higher frequency used in induction imposed to design a special plug for the inductors.

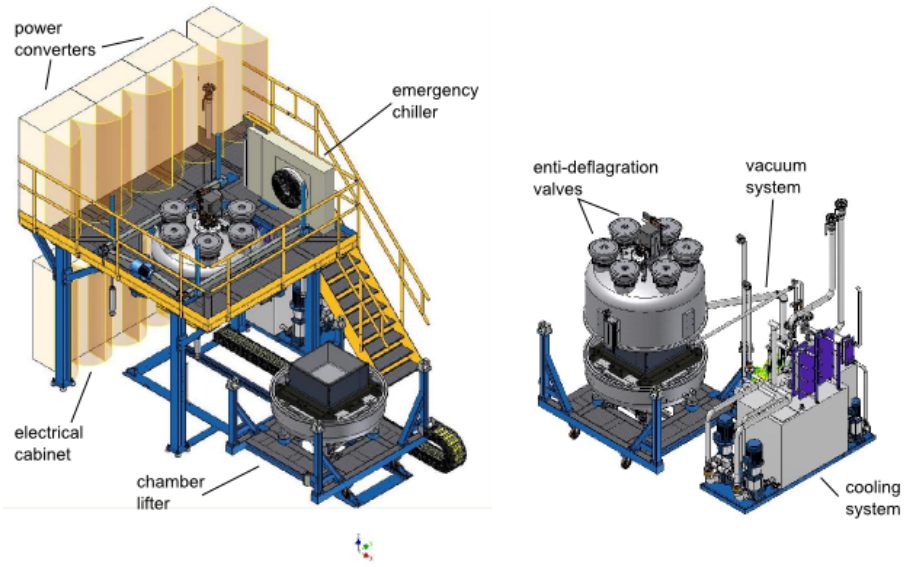

fig. 5.20: *Two views of the prototype realized displaying the main components.*

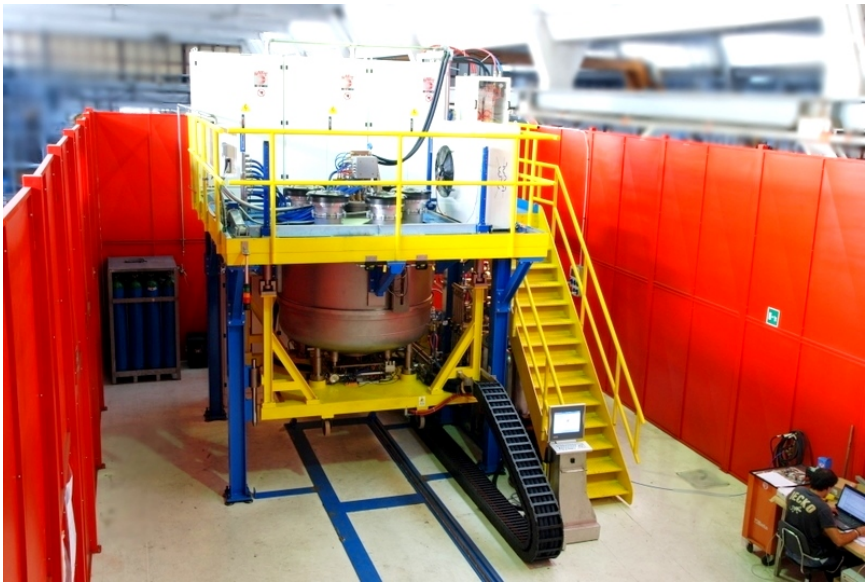

fig. 5.21: *Photo of the iDSS prototype.*

Some problems connected with **vacuum leakages** have still to be resolved.

materials

Some *materials* used in standard DSS had to be modified or completely changed due to incompatibility with the electrical inductors design: graphite felt is a perfect thermal insulation but is electrically conductive. Other

fig. 5.22: *Bottom inductor used both to heat and and cool the system.*

ceramic materials are been evaluated to replace this one. Limitation had been found in the isostatic graphite usage due to the maximum block size that can be found. The bottom susceptor has to be redesigned to utilize standard and more economical pieces.

5.3.2 Tests

The testing step started before the complete system construction in order to check some installed components. The main feaures to be controlled were **vacuum**, **inductors** matching with susceptors, and **materials** resistance to high temperarture.

Testing **power converters** gave a good concordance to the simulation's predicted values. Problems arose in the process testing phase. In certain condition power converters were shouted down due to current dispersion. Some **electric arcs** were generated inside the chamber between inductors and susceptors leaving visible effects over the graphite. Those interruptions were limited to the initial process phase when the heating process start in vacuum atmosphere in order to increase the degassing rate and increase the

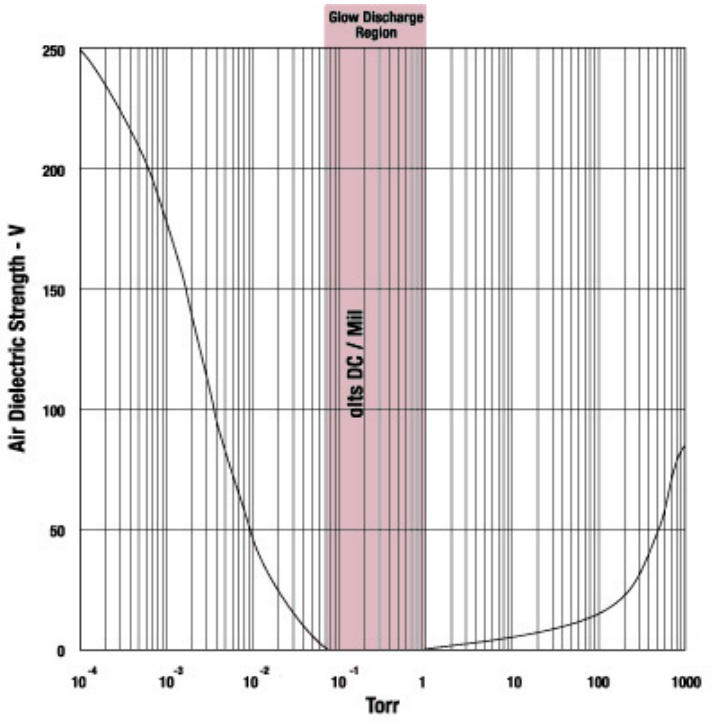

fig. 5.23: *Air dielectric strength depending on pressure and glowing discharge pressure range in evidence (1Torr ≡ 1.33mbar).*

chamber cleaning. Once identified that the possible cause was connected to vacuum level, the problem was identified as an *glow electrical discharge* caused by a drastic reduction of the air dielectric strength at low pressure as in fig.5.23. The problem has been solved switching off the power converter when the pressure is under a threshold value of 10mbar and electrically insulating all the graphite in order to set the whole structure in a floating electric potential.

glow electrical discharge

The *graphite box* containing quartz crucible has a standard design: four walls connected by CFC screws set over a graphite square base. In traditional DSS sometime a tungsten wire is used to keep them together in case of breakage. In the iDSS design the side inductor induces currents to flow from wall to wall passing the walls joint sections (graphite is normally used to realize the brush **electrical contacts** in electric motors). After some tests the joints were damaged due to scratches, dust, consumption connected to the normal walls assembling and disassembling (fig.5.24). In damaged joint points current flow finds smaller contact section with higher resistance, hence flowing through different paths (as through CFC screws and small contact

graphite box

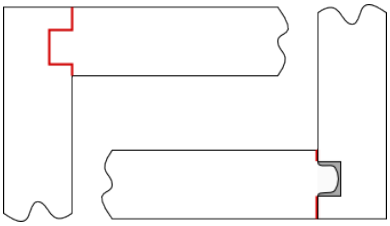

fig. 5.24: *Original and used crucible wall joint. Reducing the contact section, the current density increase.*

points), increasing temperature and creating small arc between the walls as in fig.5.25(b). The temporary solution found is to increase the screw number and tighten more by using a kind of washer in carbon felt to increase the conductive area. New box designs are being evaluated in order to realize a connection both mechanically strong and electrically conductive. The main problem is still the cost and the usability: DSS final users have to assemble and disassemble the box at each process to remove broken crucible with the ingot and put the new one with the silicon charge.

thermal shielding

A better *thermal shielding* against **reflected IR** heat fluxes has been tempted but still have to be optimize. Slits and opening for the pyrometers inspection and argon flow created direct or reflected heat exchange between susceptors and some other components not designed to resist at high temperature. Moreover, this dissipated heat flux decrease the global efficiency. Some zones have been protected using a quartz felt while some slits have been closed to reduce radiation.

The software implemented over the industrial PC controlling the DSS acquires **data** from all the devices connected. The sensors and analyzer used are:

- Type C (tungsten 5% rhenium - tungsten 26% rhenium) thermocouples, suited for measurements in the 0°C to 2320 °C range in for vacuum furnaces at extremely high temperatures
- Vacuum pressure sensors for low and high vacuum levels
- two pyrometers to measure from top (both liquid silicon or top susceptor) and a moving lateral one to check the vertical temperature profile of both susceptor or crucible through some holes made into the side insulation (fig.5.25(a))

(a)   (b)

fig. 5.25: *(a) Side pyrometer slide and quartz glasses. (b) Side box wall damaged by super-heating cause by high current concentration through the screw.*

- oxygen analyzer to check the chamber atmosphere composition and evaluate vacuum leakages
- water flow in all the system components (top and lateral inductors, and singular pancake control in the bottom one)
- water temperature in basin and in outlet of all the components
- electrical set-up for side inductor (switches, capacitors, auto-transformer, etc.)
- power converters data (frequency, voltage, current, power, power factor, etc.)
- power balance control
- global electrical power consumption
- valves and switches states

Even though some other problems are still to be resolved a first test process has been completed using a half-charged crucible with 240kg of silicon (fig.5.26).

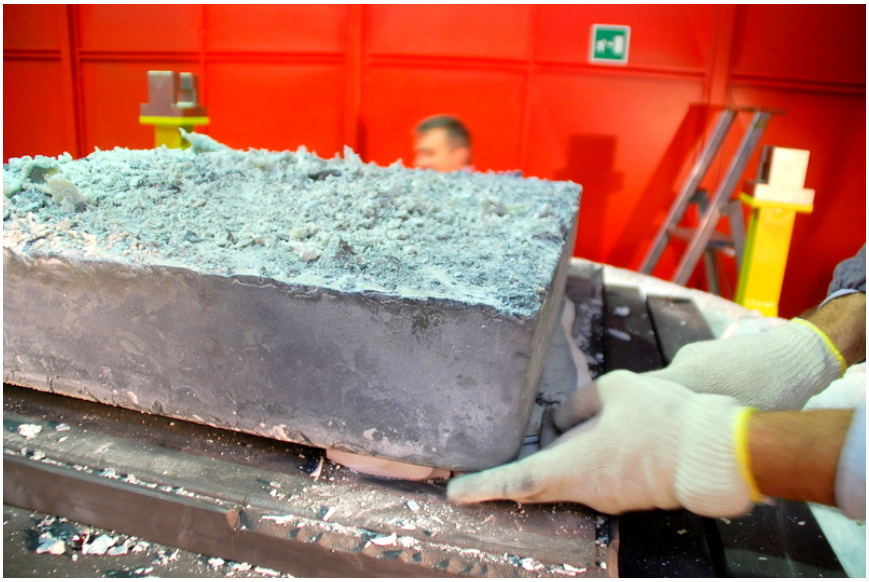

fig. 5.26: *A photo from the first ingot extraction step.*

5.3.3 Next steps

The iDSS project is still on work and lot of open points have to be analyzed:

- the **vacuum tightness** to be improved by changing the electrical feed-through,
- the gasses flow to clean the molten silicon surface. In the first ingot process a protective SiO and SiO_2 thick layer has been created reducing the thermal exchange from the top heater and cooling the melt from the top
- moreover gasses have to be used to keep clean the **quartz glasses** for the inspection and the pyrometers
- a better thermal insulation than the rigid graphite felt has to be designed to reduce heat losses and avoid electrical problems with inductors
- the thermal design and the insulation of the bottom susceptor can be redefined to reduce the cooling flux flowing to the bottom frame [61]
- the process control **software** has to be re-designed in order to be more flexible

- some additional data have to be stored in order better analyze the process flow and to be able to understand possible problems sources
- a system to check the solidification rate has to be implemented; some tricky devices have been found in literature [114]
- some mechanical components inside the chamber have to be re-designed to increase the safety in case of silicon run-out. Some groove and channel have to be relized to create preferential path to the molten silicon flowing out of the crucible

6

Conclusions and Outlook

When it is obvious
that the goals cannot be reached,
don't adjust the goals,
adjust the action steps.

Confucius

6.1 Conclusion

Due to the multi-disciplinary roots, EPM is quite a complex topic growing in theoretical research and industrial applications. To grow further, the main targets are to get together different skills and knowledge focused on the physical problem to solve, the ability to blend them and discover new

ways to apply known technologies.

The project on the γTiAl directional solidification has been developed in collaboration with the Institut für Elektroprozesstechnik of the Leibniz Universität Hannover where EPM is both a theoretical and industrial research. This project has been useful to improve the knowledge on CFD and modelization of complex phenomena such as phase changes.

Looking for new application of EPM and induction heating, the iDSS project started in 2008 with a collaboration between SAET Group and the ElectroHeat Laboratory of the University of Padova and lead to develop and realize a 450kg prototype of induction Directional Solidification System. Economical, technical, and research skills have been developed in the design and realization of the system in collaboration with industrial engineers and technicians teams.

6.2 Outlook

- the iDSS project is going on with the testing and tuning phase
- lot of improvements in thermal and fluid-dynamic aspects can be achieved
- further investigations can be done on electromagnetic stirring
- new feature of EPM can be included into the project or in similar and connected ones

Acknowledgments

The fact that we live at the bottom of a deep gravity well,
on the surface of a gas covered planet
going around a nuclear fireball 90 million miles away
and think this to be normal
is obviously some indication
of how skewed our perspective tends to be.

Douglas Adams

At first a great thanks to all the people in the iDSS project: prof. Fabrizio Dughiero and Michele Forzan, all the SAET Group and INOVA Lab teams, and prof. Sergio Pizzini. Each of them has a basic role in the whole project development and in my staying in Turin.

Thanks to all the LEP people: from prof. Sergio Lupi to all the students that made simulations for my publications ad thesis, the PhD guys, and so on.

Thank to the Institut für Elektroprozesstechnik of the Leibniz Universität in Hannover to host me for 3 months.

And at last, special thanks to all those who have contributed to this thesis remaining close to me with technical, psychological, and physical support. Even with all the skills and efforts that I could use, I would never have come this far without each one of them.

And a special thank to you.

Bibliography

[1] C. Alemany, C. Trassy, B. Pateyron, K. I Li, and Y. Delannoy. Refining of metallurgical-grade silicon by inductive plasma. *Solar Energy Materials and Solar Cells*, 72(1-4):4148, 2002.

[2] D.V. Alexandrov, D.L. Aseev, I.G. Nizovtseva, H.-N. Huang, and D. Lee. Nonlinear dynamics of directional solidification with a mushy layer. analytic solutions of the problem. *International Journal of Heat and Mass Transfer*, 50(17-18):3616–3623, August 2007.

[3] Vasilios Alexiades and Alan D. Solomon. *Mathematical Modeling of Melting and Freezing Processes*. Taylor & Francis, 1993.

[4] T. Ando, K. Ueno, Shoji TANIGUCHI, and T. Takagi. Visual system experiment of MHD pump using rotating twisted magnetic field applicable to High-Temperature molten metals. *ISIJ Int (Iron Steel Inst Jpn)*, 43(6):849–854, 2003.

[5] T. Ando, K. Ueno, Shoji TANIGUCHI, and T. Takagi. Induction pump for high-temperature molten metals using rotating twisted magnetic field: molten gallium experiment. *IEEE transactions on Magnetics*, 40(4):1846–1857, July 2004.

[6] S. Asai. Recent development and prospect of electromagnetic processing of materials. *Science and Technology of Advanced Materials*, 1(4):191–200, December 2000.

[7] S. Asai. ELECTROMAGNETIC PROCESSING OF MATERIALS, PAST, PRESENT AND FUTURE. *Advanced Processing of Metals and Materials: New, improved and existing technologies: iron and steel: recycling and waste treatment*, page 205, 2006.

[8] Shigeo Asai. Recent activities on electromagnetic processing of materials in nagoya university. In *Proceedings of Modeling for Electromagnetic Processing 2003*, Hannover, March 2003.

[9] B. R. Bathey and M. C. Cretella. Solar-grade silicon. *Journal of Materials Science*, 17(11):3077–3096, November 1982.

[10] C. Beckermann, H. -J. Diepers, I. Steinbach, A. Karma, and X. Tong. Modeling melt convection in Phase-Field simulations of solidification. *Journal of Computational Physics*, 154(2):468–496, September 1999.

[11] V. Berdnikov, M. Filippova, B. Krasin, and A. Nepomnyashchikh. Numerical simulation of thermal-physical processes accompanying multisilicon crystal growing by the method of bridgman stockbarger. *Thermophysics and Aeromechanics*, 13(2):257–274, 2006.

[12] A. Bermudez, D. Gmez, M. C. Muiz, P. Salgado, and R. Vzquez. Numerical simulation of induction furnaces for silicon purification. *Progress in Industrial Mathematics at ECMI 2006*, 12(1):48–65, 2008.

[13] A. Bermudez, R. Leira, M.C. Muiz, and F. Pena. Numerical modelling of a transient conductive-radiative thermal problem arising in silicon purification. *Finite Elements in Analysis and Design*, 42(10):809–820, June 2006.

[14] J. Blazek. *Computational Fluids Dynamics*. Elsevier, 2001.

[15] V. Bojarevics and K. Pericleous. AC & DC magnetic levitation and semi-levitation modelling. In *Proceedings of Modeling for Electromagnetic Processing 2003*, Hannover, March 2003.

[16] V. Bojarevics, K. Pericleous, and M. Cross. Modeling the dynamics of magnetic semilevitation melting. *Metallurgical and Materials Transactions B*, 31(1):179–189, 2000.

[17] C.A. Borghi, A. Cristofolini, and M. Fabbri. Study of the design model of a liquid metal induction pump. *Magnetics, IEEE Transactions on*, 34(5):2956–2959, 1998.

[18] A.F.B. Braga, S.P. Moreira, P.R. Zampieri, J.M.G. Bacchin, and P.R. Mei. New processes for the production of solar-grade polycrystalline silicon: A review. *Solar Energy Materials and Solar Cells*, 92(4):418–424, April 2008.

[19] M. Bruncko, I. Anzel, and A. Krizman. Monitoring of directional solidification with simultaneous measurements of electrical resistance and temperature. *Materials Characterization*, 51(2-3):185–199, October 2003.

[20] L. C. Burton and A. H. Madjid. Coulomb screening in intrinsic Medium-Gap semiconductors and the electrical conductivity of silicon at elevated temperatures. *Physical Review*, 185(3):1127, 1969. Copyright (C) 2009 The American Physical Society.

[21] Alok Choudhury, Matthias Blum, Harald Scholz, and Georg Jarczyk. Method and apparatus for the oriented solidification of molten silicon to ..., February 2000. U.S. Classification: 117/18; 117/33; 117/214; 117/216; 117/924 ; International Classification: C30B 1520.

[22] Shravan Kumar Chunduri. Crystallizing silicon: market survey on crystal growth equipment. *Photon International*, 2009/6:154 – 171, June 2009.

[23] Shravan Kumar Chunduri. Bigger and better - and retro? *Photon International*, 2010/6:184–208, June 2010.

[24] Dario Ciscato, E. Baake, A. Jakovics, and A. Umbrashko. Numerical investigation of TiAl meeting and solidification in induction furnace with cold crucible. In *Proceedings of 6th international conference on electromagnetic processing of materials - EPM 2009*, page 517520, DRESDEN, October 2009. Forschungszentrum Dresden-Rossendorf.

[25] Dario Ciscato, Fabrizio Dughiero, and Michele Forzan. A comparison between resistance and induction DSS furnaces for solar grade silicon production. In *Proceedings of the 6th International Conference on electromagnetic processing of materials - EPM 2009*, Dresden, October 2009.

[26] Dario Ciscato, Fabrizio Dughiero, Michele Forzan, and Cristiano Greggio. MHD FEM analysis of electromagnetic stirrers for aluminum furnaces. In *12th Biennial IEEE Conference on Electromagnetic Field Computation - 2006*, page 319, Miami, FL (USA), May 2006.

[27] Dario Ciscato, Michele Forzan, and Fabrizio Dughiero. A new DSS furnace for energy saving in the production of multi-crystalline silicon. In *35th IEEE Photovoltaic Specialists Conference*, Honolulu (Hawaii), 2010. IEEE.

[28] T.F. Ciszek. siliconsultant.com. http://www.siliconsultant.com/, 2010.

[29] T.F. Ciszek, Guenter H. Schwuttke, and K. H. Yang. Solar-Grade silicon by directional solidification in carbon crucibles. *Energy Technology*, 23(3):270, May 1979.

[30] Theodore F. Ciszek and Jeffery L. Hurd. Apparatus for melt growth of crystalline semiconductor sheets, June 1986. undefinedFiling Date: Feb 25, 1981 U.S. Classification: 422/246 International Classification: C30B 1534.

[31] Theodore F. Ciszek and Guenter H. Schwuttke. Method and apparatus for drawing monocrystalline ribbon from a melt, November 1981. undefinedFiling Date: Aug 20, 1980 U.S. Classification: 156/608 International Classification: C30B 1534.

[32] G. Coletti, L. J. Geerligs, P. Manshanden, C. Swanson, S. Riepe, W. Warta, J. Arumughan, and R. Kopecek. Impact of iron and molybdenum in mono and multicrystalline float-zone silicon solar cells. *Solid State Phenomena*, 131:1520, 2008.

[33] G. Coletti, R. Kvande, V. D. Mihailetchi, L. J. Geerligs, L. Arnberg, and E. J. Øvrelid. Effect of iron in silicon feedstock on p- and n-type multicrystalline silicon solar cells. *Journal of applied physics*, 104(10):104913, 2009.

[34] Gianluca Coletti. Silicon feedstock: options and specifications. In *Presented at the CrystalClear Final Event*, Munich (Germany), May 2009.

[35] Daniel Cook, Yitung Chen, Lillian Ratliff, Huajun Chen, and Jian Ma. Numerical modeling do EM pump efficiency. In *Proceedings of International Engineering Congress and Exposition*, Chicago, IL, November 2006.

[36] Dominique Coupard, Thierry Palin-luc, Philippe Bristiel, Vincent Ji, and Christian Dumas. Residual stresses in surface induction hardening of steels: Comparison between experiment and simulation. *Materials Science and Engineering: A*, 487(1-2):328–339, 2008.

[37] A. Cuevas. The paradox of compensated silicon. In *Optoelectronic and Microelectronic Materials ad Devices*, pages 238—241, Sydney, July 2008.

[38] J. Degoulange, I. Perichaud, C. Trassy, and S. Martinuzzi. Multicrystalline silicon wafers prepared from upgraded metallurgical feedstock. *Solar Energy Materials and Solar Cells*, 92(10):1269–1273, October 2008.

[39] C. del Caizo, G. del Coso, and W.C. Sinke. Crystalline silicon solar module technology: Towards the 1euro per watt-peak goal. *Progress in Photovoltaics: Research and Applications*, 17(3):199–209, 2009.

[40] Y. Delannoy. ELECTROMAGNETIC PROCESSING OF MATERIALS: FROM THE CONCEPTS TO INDUSTRIAL APPLICATIONS. In *Materials Processing in Magnetic Fields - Proceedings of the International Workshop on Materials Analysis and Processing in Magnetic Fields*, pages 169–177, Tallahassee, Florida, 2005.

[41] H. Ding, R. Chen, Y. Wang, H. Fu, J. Guo, W. Bi, and J. Jia. Continuous casting and directional solidication of titanium alloys with cold crucible. *Materials science forum*, 475-47(4):2575, 2005.

[42] Hongsheng Ding, Ruirun Chen, JingJie Guo, Weisheng Bi, Daming Xu, and HengZhi Fu. Directional solidication of titanium alloys by electromagnetic connement in cold crucible. *Materials Letters,*, 59(7):741–745, 2005.

[43] Vishu D. Dosaj and Lee P. Hunt. Method for producing solar-cell-grade silicon, January 1981. U.S. Classification: 423/350; 156/616R; 23296 ; International Classification: C01B 3302.

[44] Thierry Duffar, Carmen Stelian, and A. Mitric. Effect of magnetic field in bridgman growth of semiconducto alloys. In *Proceedings of Modeling for Electromagnetic Processing 2003*, Hannover, March 2003.

[45] Fabrizio Dughiero, Michele Forzan, and Sergio Lupi. Reheaing 150mm billets of a356 alloy for thixo-processing. In *Proceedings of Modeling for Electromagnetic Processing 2003*, Hannover, March 2003.

[46] Fabrizio Dughiero, Sergio Lupi, and Enrico Tittonel. Analysis of a laboratory prototype of longitudinal electromagnetic levitator. In *Proceedings of Modeling for Electromagnetic Processing 2003*, Hannover, March 2003.

[47] E. Ehret. Characterization of multicrystalline silicon:: Comparison between conventional casting and electromagnetic casting processes. *Solar Energy Materials and Solar Cells*, 53(3-4):313–327, 1998.

[48] R. Einhaus, J. Kraiem, F. Cocco, Y. Caratini, D. Bernou, D. Sarti, G. Rey, R. Monna, C. Trassy, and J. Degoulange. PHOTOSIL - simplified production of solar silicon from metallurgical silicon. In *21th European Photovoltaic Solar Energy Conference*, Dresden, September 2006.

[49] R. Einhaus, D. Sarti, C. Hassler, C. Trassy, Y. Delannoy, S. De Wolf, F. Ferrazza, S. Martinuzzi, and W. Warta. Purification of low quality silicon feedstock [for solar cell fabrication]. In *Photovoltaic Specialists Conference, 2000. Conference Record of the Twenty-Eighth IEEE*, pages 221–224, 2000.

[50] Roland Einhaus, Francois Lissalde, and Pascal Rivat. Crucibel for a device used for the production of a block of crystalline material, and production method, July 2006.

[51] EU. Road map for renewable energy in europe. European Parliament Resolution INI/2007/2090, European Parliament, September 2007.

[52] Ivar Farup and Asbjorn Mo. Two-phase modeling of mushy zone parameters associated with hot tearing. *Metallurgical and Materials Transactions A*, 31(5):1461–1472, 2000.

[53] Joel H. Ferziger and M. Peric. *Computational methods for uid dynamics*. Springer, 3 edition, 2002.

[54] Oleg S. Fishman. Solar silicon, part i. *Advanced Materials & Processes*, 166(9):39–40, September 2008.

[55] Oleg S. Fishman. Solar silicon, part II. *Advanced Materials & Processes*, 166(10):33–34, October 2008.

[56] E. Fourmond, C. Ndzogha, D. Pelletier, Y. Delannoy, C. Trassy, Y. Caratini, Y. Baluais, R. Einhaus, S. Martinuzzi, and I. Prichaud. Refining of metallurgical silicon for crystalline solar cells. In *Proceedings of the 19th European Photovoltaic Solar Energy Conference, Paris*, volume 7, 2004.

[57] D. Franke, T. Rettelbach, C. Hasler, W. Koch, and A. Muller. Silicon ingot casting: process development by numerical simulations. *Solar Energy Materials and Solar Cells*, 72(1-4):83–92, April 2002.

[58] K. Fujiwara, W. Pan, K. Sawada, M. Tokairin, N. Usami, Y. Nose, A. Nomura, T. Shishido, and K. Nakajima. Directional growth method to obtain high quality polycrystalline silicon from its melt. *Journal of Crystal Growth*, 292(2):282–285, 2006.

[59] W. Fulkerson, J. P. Moore, R. K. Williams, R. S. Graves, and D. L. McElroy. Thermal conductivity, electrical resistivity, and seebeck coefficient of silicon from 100 to 1300K. *Physical Review*, 167(3):765, March 1968. Copyright (C) 2009 The American Physical Society.

[60] L. J. Geerligs, P. Manshanden, G. P. Wyers, E. J. Ovrelid, O. S. Raaness, A. N. Waernes, and B. Wiersma. Specification of solar grade silicon: how much common impurities affect the cell efficiency of MC-Si solar cells. In *Proceedings of the 20th European Photovoltaic Solar Energy Conference and Exhibition*, Barcelona, Spain, June 2005.

[61] Francesco Giusto. Numerical analysis of unidirectional ingot casting processes for multi-crystalline silicon solar cells. Master's thesis, Universitá degli Studi di Padova, Padova, 2009.

[62] J. Gnauk, R. Wenke, and G. Frommeyer. Macroscopic modeling of solidification processes by performing the generalized enthalpy method. *Materials Science and Engineering: A*, 413-414:490–496, December 2005.

[63] GrafTech. THE INDUSTRIAL GRAPHITE ENGINEERING HANDBOOK. Product catalogue properties, UCAR Carbon Company Inc., 2004.

[64] M. Hainke, J. Friedrich, D. Vizman, and G. Mller. MHD effects in semiconductor crystal growth and alloy solidification. In *Proceedings of Modeling for Electromagnetic Processing 2003*, Hannover, March 2003.

[65] J. Hofstetter, J.F. Lelivre, C. del Caizo, and A. Luque. Acceptable contamination levels in solar grade silicon: From feedstock to solar cell. *Materials Science and Engineering: B*, In Press, Corrected Proof, March 2009.

[66] Fluent Inc. Fluent, 2006.

[67] N. Jekabson, A. Jakovics, and V. V. Na. Model of protective (Skull) layer in the Inductor-Crucible furnace. In *Proceedings of Modeling for Electromagnetic Processing 2003*, Hannover, March 2003.

[68] K. Kaneko, T. Misawa, and K. Tabata. Cold crucible induction casting of semiconductor silicon for solar cell. In *Photovoltaic Specialists Conference, 1990., Conference Record of the Twenty First IEEE*, pages 674–677 vol.1, 1990.

[69] Kyojiro Kaneko, D. Landau, and P. Gillon. Cost estimates of silicon manufacture by metallurgy. *Photovoltaics Bulletin*, 2002(12):8–10, 2002.

[70] Kyojiro Kaneko and Jun-Ya Masuda. Apparatus for casting silicon with gradual cooling, April 1990. undefinedFiling Date: 30 Jun 1989 U.S. Classification: 65144; International Classification: C03B 3702.

[71] Kyojiro Kaneko and Hideyuki Mizumoto. Method of manufacturing single-crystal silicon, December 1993. U.S. Classification: 156/617.1; 156/618.1; 156/620.4; 156DIG83; 156DIG102; 156DIG103 ; International Classification: C30B 2906.

[72] Ch. Karcher, V. Kocourek, and D. Schulze. Experimental investigations of electromagnetic instabilities of free surfaces in a liquid metal drop. In *Proceedings of Modeling for Electromagnetic Processing 2003*, Hannover, March 2003.

[73] H. Kasjanow, Alexander Nikanorov, B. Nacke, H. Behnken, D. Franke, and Albrecht Seidl. 3D coupled electromagnetic and thermal modeling of EFG silicon tube growth. *Journal of Crystal Growth*, 303(1):175 – 179, May 2007.

[74] Lawrence L. Kazmerski. Solar photovoltaics R&D at the tipping point: A 2005 technology overview. *Journal of Electron Spectroscopy and Related Phenomena*, 150(2-3):105–135, February 2006.

[75] Lawrence L. Kazmerski. NREL compilation of best research solar cell efficiencies. Plot, NREL, September 2010. http://upload.wikimedia.org/wikipedia/commons/7/74/PVeff(rev100921).jpg.

[76] R. M. Khristinich, M. V. Pervukhin, V. V. Stafievskaya, and T. A. Boyakova. Electromagnetic devices for setting up moltem metal circulation. In *Proceedings of Modeling for Electromagnetic Processing 2003*, Hannover, March 2003.

[77] R. M. Khristinich, V. N. Timofeyev, V. V. Stafievskaya, and A. V. Valenteyekno. Molten metal electromagnetic stirring in metallurgy. In *Proceedings of Modeling for Electromagnetic Processing 2003*, Hannover, March 2003.

[78] J. Kraiem, B. Drevet, F. Cocco, N. Enjalbert, S. Dubois, D. Camel, D. Grosset-Bourbange, D. Pelletier, T. Margaria, and R. Einhaus. High performance solar cells made from 100% UMG silicon obtained via the PHOTOSIL process. In *Photovoltaic Specialists Conference (PVSC), 2010 35th IEEE*, pages 001427–001431, 2010.

[79] J. Kraiem, R. Einhaus, F. Lissalde, S. Dubois, N. Enjalbert, B. Drevet, F. Servant, and D. Camel. Innovative crystallisation of Multi-Crystalline silicon ingots from different types of silicon feedstock. In *Proc. of 23th European PV Solar Energy Conference*, page 10711074, Valencia, 2008.

[80] Armands Krauze, Andris Muiznieks, A. Mhlbauer, Thomas Wetzel, and Janis Virbulis. Numerical 3D modelling of turbulent melt flow in CZ system with horizontal DC megnatic field. In *Proceedings of Modeling for Electromagnetic Processing 2003*, Hannover, March 2003.

[81] Rannveig Kvande, yvind Mjs, and Birgit Ryningen. Growth rate and impurity distribution in multicrystalline silicon for solar cells. *Materials Science and Engineering: A*, 413-414:545–549, December 2005.

[82] Xi Li, Annie Gagnoud, Zhongming Ren, Yves Fautrelle, and Rene Moreau. Investigation of thermoelectric magnetic convection and its effect on solidification structure during directional solidification under a low axial magnetic field. *Acta Materialia*, 57(7):2180–2197, April 2009.

[83] J. Libal, S. Novaglia, M. Acciarri, S. Binetti, R. Petres, J. Arumughan, R. Kopecek, and A. Prokopenko. Effect of compensation and of metallic impurities on the electrical properties of cz-grown solar grade silicon. *Journal of applied physics*, 104(10):104507, 2009.

[84] F. Lissalde, Roland Einhaus, J. Kraiem, and B. Debunne. Innovative crystallization process and furnace for solar grade silicon. In *22nd EUPVSEC*, pages 948–951, Valencia, 2007.

[85] Lijun Liu, Satoshi Nakano, and Koichi Kakimoto. An analysis of temperature distribution near the melt-crystal interface in silicon czochralski growth with a transverse magnetic field. *Journal of Crystal Growth*, 282(1-2):49–59, August 2005.

[86] LiangShun Luo, YanQing Su, JingJie Guo, Xinzhong Li, and HengZhi Fu. A simple model for lamellar peritectic coupled growth with peritectic reaction. *Science in China Series G: Physics Mechanics and Astronomy*, 50(4):442–450, 2007.

[87] Wenzhong Luo, Jun Shen, Zhixian Min, and HengZhi Fu. Lamellar orientation control of TiAl alloys under high temperature gradient with a Ti-43Al-3Si seed. *Journal of Crystal Growth*, 310(24):5441–5446, 2008.

[88] Sergio Lupi. Heating by internal sources 2001. Conference proceedings, Dip. Ingegneria Elettrica, Universitá degli Studi di Padova, Padova, 2001.

[89] Jaroslav Mackerle. Finite element analysis and simulation of quenching and other heat treatment processes: A bibliography (1976-2001). *Computational Materials Science*, 27(3):313–332, 2003.

[90] Carlo Mapelli. Simulation of the electromagnetic stirrers and brakes applied in the metallurgical field. In *Excerpt from COMSOL Users Conference*, Milano, 2006.

[91] Mitsumasa Mito, Takao Tsukada, Mitsunori Hozawa, Chiaki Yokoyama, You-Rong Li, and Nobuyuki Imaishi. Sensitivity analuses of the thermophysical properties of silicon melt and crystal. *Measurement Science and Technology*, 16(2):457 – 466, 2005.

[92] Hiroaki Miyazawa, Lijun Liu, and Koichi Kakimoto. Numerical analysis of influence of crucible shape on interface shape in a unidirectional solidification process. *Journal of Crystal Growth*, 310(6):1142—114, 2008.

[93] H. K. Moffat. Electromagnetic stirring. *Physics o Fluids A*, 3(5):1336–1343, May 1991.

[94] H.J. Moller, C. Funke, M. Rinio, and S. Scholz. Multicrystalline silicon for solar cells. *Thin Solid Films*, 487(1-2):179–187, September 2005.

[95] Sergei Molokov, Chris Reilly, Yves Lion, and Roberto Caciuffo. 161st CSO meeting - proposal for a new COST action. Memorandum of understanding, European Cooperation in Science and Technology, March 2005.

[96] A. Müller, M. Ghosh, R. Sonnenschein, and P. Woditsch. Silicon for photovoltaic applications. *Materials Science and Engineering: B*, 134(2-3):257–262, 2006.

[97] Tetsuo Munakata and Ichiro Tanasawa. Study on silicon melt convection during the RF-FZ crystal growth process: I. experimental ow visualization. *Journal of Crystal Growth,*, 206(1-2):23–26, 1999.

[98] Katsumi Nakagawa, Shunichi Ishihara, Hiroshi Sato, and Shoji Nishida. Continuous production method for crystalline silicon and production ..., March 2005. U.S. Classification: 117018000; 117208000; 117214000 ; International Classification: C30B015/00; C30B021/06; C30B027/02; C30B028/10; C30B030/04.

[99] Keita Nakagawa, Tomohiro Onizuka, Ken ichi Sasatani, Nobuyuki Kubo, and Michio Kida. Manufacturing of silicon ingot by electromagnetic casting. In *5th international symposium on Electromagnetic Processing of Materials*, Sendai (Japan), 2006. ISIJ.

[100] N. Nigro, A. Huespe, and V. Fachinotti. Phasewise numerical integration of finite element method applied to solidification processes. *International Journal of Heat and Mass Transfer*, 43(7):1053–1066, April 2000.

[101] E. J. Øvrelid, E. Olsen, Martin Syvertsen, Birgitte Karlsen, and M. de Sabatino. Directional crystallisation of high quality silicon ingots, January 2008.

[102] Sorin Pasca. PARTICULARITIES ON NUMERICAL MODELING OF CRUCIBLE INDUCTION FURNACE. *Revue Roumaine des Sciences Techniques*, 49(4), 2004.

[103] J. Perlin. Silicon solar cell turns 50. Technical report, National Renewable Energy Lab., Golden, CO.(US), 2004.

[104] S. Pizzini, M. Acciarri, and S. Binetti. From electronic grade to solar grade silicon: chances and challenges in photovoltaics. *physica status solidi (a)*, 202(15):2928–2942, 2005.

[105] Gundars Ratnieks, Andris Muiznieks, and Alfred Muhlbauer. Mathematical modelling od industrial FZ process for large (200mm) silicon crystal growth. In *Proceedings of Modeling for Electromagnetic Processing 2003*, Hannover, March 2003.

[106] Paolo Redi. Polysilicon: production technologies and market outlook. *PV International*, pages 36–42, March 2009.

[107] Alan Ristow and Ajeet Roha. Analytical modeling of the relationship between photovoltaic module manufacturing cost and power conversion efficiency. In *16th Workshop on Crystalline Silicon Solar Cells and Modules: Materials and Processes - Extended Abstracts and Papers*, pages 206–210, Denver (Colorado), August 2006. NREL.

[108] S. Rousseau, M. Benmansour, D. Morvan, and J. Amouroux. Purification of MG silicon by thermal plasma process coupled to DC bias of the liquid bath. *Solar Energy Materials and Solar Cells*, 91(20):1906–1915, 2007.

[109] Emanuel M. Sachs. Melt dumping in string stabilized ribbon growth, December 1986. undefinedFiling Date: Nov 5, 1982 U.S. Classification: 156/608 International Classification: C30B 1500.

[110] Emanuel M. Sachs. String stabilized ribbon growth, April 1987. undefinedFiling Date: Jan 7, 1980 U.S. Classification: 156/616R International Classification: C30B 1102; C30B 1534; B01D 900.

[111] Dominique Sarti and Roland Einhaus. Silicon feedstock for the multi-crystalline photovoltaic industry. *Solar Energy Materials and Solar Cells*, 72(1-4):27–40, April 2002.

[112] H. R. Shanks, P. D. Maycock, P. H. Sidles, and G. C. Danielson. Thermal conductivity of silicon from 300 to 1400K. *Physical Review*, 130(5):1743, 1963. Copyright (C) 2009 The American Physical Society.

[113] Carissa Smith and Andrew Barron. Syntesis and purification of bulk semiconductors, September 2009. `http://cnx.org/content/m23936/1.5/`.

[114] Anne Karin; Søiland. *Silicon for Solar Cells*. PhD dissertation, Norwegian University of Science and Technology, 2005.

[115] Bhushan Sopori. 16th workshop on crystalline silicon solar cells and modules: materials and processes; extended abstracts and papers. Workshop proceedings, NREL, Denver (Colorado), August 2006.

[116] YanQing Su, Chang Liu, Xinzhong Li, JingJie Guo, Bangsheng Li, Jun Jia, and HengZhi Fu. Microstructure selection during the directionally peritectic solidication of TiAl binary system. *Intermetallics,*, 13(3-4):267–274, 2005.

[117] J. Suhm, M. Moeller, and H. Linn. New development for industrial microwave heating. In *Proceedings of Modeling for Electromagnetic Processing 2003*, Hannover, March 2003.

[118] Dawei Sun, Chenlei Wang, Hui Zhang, Brian Mackintosh, Doug Yates, and Juris Kalejs. A multi-block method and multi-grid technique for large diameter EFG silicon tube growth. *Journal of Crystal Growth*, 266(1-3):167–174, 2004.

[119] T. Takakura and S. Kidoguchi. Effect of rapid thermal process for CDS silicon solar cell. In *Proceeding of the 23rd European PhotoVoltaic Solar Energy Conference and Exhibition*, pages 1472 – 1474, Valencia, Spain, September 2008.

[120] Ying-Yang Teng, Jyh-Chen Chen, Chung-Wei Lu, and Chi-Yung Chen. The carbon distribution in multicrystalline silicon ingots grown using the directional solidification process. *Journal of Crystal Growth*, 312(8):1282–1290, April 2010.

[121] C. Trassy, J. Kraiem, Y. Delannoy, Roland Einhaus, Y. Caratini, D. Bernou, and P. Rivat. PHOTOSIL: an industrial pilot combining inductive plasma, inductive stirring and controlled solidification for material processing. In *5th international symposium on Electromagnetic Processing of Materials*, Sendai (Japan), 2006. ISIJ.

[122] R. van Overstraeten, R. Mertens, and J. Nijs. Progress in photovoltaic energy conversion. *Rep. Prog. Phys*, 45:1041–1108, 1982.

[123] Dieter Weidhaus and Alexander Hayduk. Radiation-heated fluidized-bed reactor, April 2006. Date: Oct 2, 2000 U.S. Classification: 422/139.

[124] James Werner and Harold Adkins. Electromagnetic pump fabrication and predicted performance. In *Proceedings of Nuclear and Emerging Technologies for Space 2009*, Atlanta (GA), June 2009.

[125] E. Wrona, B. Nacke, and D. Resetov. 3D-modelling of the transient heating process for induction surface hardening. In *Proceedings of Modeling for Electromagnetic Processing 2003*, Hannover, March 2003.

[126] Bei WU, Nathan Stoddard, Ronghui Ma, and Roger Clark. Bulk multicrystalline silicon growth for photovoltaic (PV) application. *Journal of Crystal Growth*, 310(7-9):2178–2184, April 2008.

[127] V. V. Yakovlev. Efficient electromagnetic models for systems and processes of microwave heating. In *Proceeding of Heating by Interal Sources 2001*, Padova, 2001.

[128] M. Yamaguchi, D. R. Johnson, H. N. Lee, and H. Inui. Directional solidification of TiAl-base alloys. *Intermetallics*, 8(5-6):511–517, May 2000.

[129] Kouji Yasuda and Toru H. Okabe. Solar-grade silicon production by metallothermic reduction. *JOM*, 62(12):94–101, 2010.

[130] N. Yuge, M. Abe, K. Hanazawa, H. Baba, N. Nakamura, Y. Kato, Y. Sakaguchi, S. Hiwasa, and F. Aratani. Purification of metallurgical-grade silicon up to solar grade. *Progress in Photovoltaics: Research and Applications*, 9(3):203–209, 2001.

[131] A. Yvon, E. Fourmond, C. Ndzogha, Y. Delannoy, and C. Trassy. Inductive plasma process for refining of solar grade silicon. In *Heating by Electromagnetic Sources*, Padova, 2000.

[132] Zhenni Zhou, Guohong Zhan, and Kaiming Wu. Effect of strong magnetic field on isothermal transformation of degenerate pearlite in an Fe-C-Mo alloy. *Acta Metallurgica Sinica*, 23(4):248–254, 2010.

[133] Olgierd Cecil Zienkiewicz and Robert Lee Taylor. *Finite Element Method: Fluid Dynamics*, volume 3. Butterworth Heinemann, 2000.

[134] Olgierd Cecil Zienkiewicz and Robert Lee Taylor. *Fluid dynamics*, volume 3. Butterworth Heinemann, 2000.

[135] Werner Zulehner. Historical overview of silicon crystal pulling development. *Materials Science and Engineering B*, 73(1-3):7–15, April 2000.